

Disentangling the chemistry and transport impacts of the Quasi-Biennial Oscillation on stratospheric ozone

Jinbo Xie^{1#}, Qi Tang¹, Michael Prather², Jadwiga Richter³, Shixuan Zhang⁴

¹Lawrence Livermore National Laboratory, Livermore, CA, USA

²Department of Earth System Science, University of California, Irvine, CA, USA

³National Center for Atmospheric Research, Boulder, CO, USA

⁴Pacific Northwest National Laboratory, Richmond, WA, USA

[#]now at Princeton University, New Jersey, NJ, USA

Correspondence to: Jinbo Xie (jinbo.xie@princeton.edu)

Abstract

The quasi-biennial oscillation (QBO) in tropical winds perturbs stratospheric ozone throughout much of the atmosphere via changes in transport of ozone and other trace gases and temperature changes, all of which alter ozone chemistry. Attributing these causes of the QBO-ozone variability may provide insight to model-to-model differences that contribute to ozone simulation. Here we develop a novel metric of steady-state ozone (SSO) to separate these effects: SSO calculates the local steady-state response of ozone due to the changes in temperature, chemical species, and overhead ozone column; the response due to circulation change is presumed when SSO shown no response. It is applied to the nudged Department of Energy's Energy Exascale Earth System Model version 2 (E3SMv2) with interactive ozone chemistry to demonstrate its validity. The E3SMv2 simulations nudged to reanalysis data produced reasonable wind and ozone patterns especially in the Tropics. Consistent with previous studies, we find clear demarcations with pressure. Ozone perturbations in the upper stratosphere (< 6 hPa) are predicted by the temperature changes; those between 6-hPa to 20-hPa are predicted by NO_y changes; and those in the lower stratosphere show no temperature or NO_y response and are presumably driven by circulation changes. These results are important for diagnosing model-to-model discrepancy in QBO-ozone response and enhancing reliability of ozone projections.

Deleted: xie7@llnl.gov

Deleted: , now at Princeton University (jinbo.xie@princeton.edu)...

Formatted: Indent: First line: 0"

Deleted: via

Deleted: examine these changes using

Deleted: linearized stratospheric

Moved (insertion) [2]

Deleted: With an offline version of our stratospheric chemistry module we calculate the local steady-state response of tropical ozone to the modeled changes temperature, chemical species, and overhead ozone column, and develop new diagnostics for QBO studies with interactive chemistry.

Moved up [2]: With an offline version of our stratospheric chemistry module we calculate the local steady-state response of tropical ozone to the modeled changes temperature, chemical species, and overhead ozone column, and develop new diagnostics for QBO studies with interactive chemistry.

Deleted: produces a natural QBO cycle in winds, temperature, and ozone. Our analysis identifies climatological QBO patterns of ozone for the period 1979-2020 using both nonlinear principal component analysis and monthly composites centered on the QBO phase transition month. As a free-running climate model, E3SM's QBO does not synchronize with the observed QBO, but it does match the climatological phasing of the observed patterns.

Deleted:

Deleted: Diagnostics that separate chemistry vs. transport driven changes in ozone provide insight into model differences in simulating the QBO.

1. Introduction

The Quasi-Biennial Oscillation (QBO) is the principal mode of dynamical variability in the stratosphere. It is the key source of interannual variability in the overall chemical composition of the stratosphere (Randel et al., 1998; Shuckburgh et al. 2001; Park et al. 2017), manifest primarily through ozone (Reed 1964; Bowman, 1989; Wang et al., 2022).

The QBO affects ozone through both transport via atmospheric circulation and chemical processes via changed composition of the atmosphere (Reed, 1964; Holton et al., 1989; Gray and Dunkerton, 1990; Chipperfield and Gray, 1992; Chipperfield et al., 1994, Politowicz and Hitchman, 1997; Jones et al., 1998; Baldwin et al., 2001). The alternate change of QBO phase speeds up and slows down the vertical ascent in the tropics that pushes the ozone profile up and down; the QBO-temperature warms and cools the stratosphere that accelerates and decelerates ozone cycle; QBO-associated vertical transport of trace gas like reactive nitrogen reservoir NO_y may also affect ozone cycle.

Disentangling these causes of QBO-ozone variability is useful to understanding model-to-model discrepancy in the QBO-ozone simulation that contributes to improved ozone projections, such as the rate of ozone recovery that is still accompanied by large uncertainty due to internal climate variabilities like QBO (Chipperfield et al., 2017; Stone et al., 2018). Yet the role of chemical and dynamic process on QBO-ozone is still under debate (Zhang et al., 2021). Ling and London (1986) pointed to a close relationship between ozone and QBO-induced temperature anomaly and its associated photochemistry above 15-hPa. Chipperfield et al. (1994) and Tian et al. (2006) attribute the QBO-ozone to QBO modulation of NO_y species rather than the temperature changes above 10–15-hPa. Butchart et al., (2003), on the other hand, used a 3-D chemistry-climate model to argue that the transport is as important above 15–20-hPa. Currently, challenges in attributing QBO-ozone variability remain due to co-existent of chemistry and transport impact (Baldwin et al, 2001), and model limitations in simulating a free-running QBO variability (Richter et al., 2020) including asymmetry between QBO phases – a stronger and shorter QBO easterly phase and weaker and longer QBO westerly phase (Scaife et al., 2014; Richter et al., 2020). To separate the co-existent impacts, we built upon a novel use of the steady-state ozone (SSO) metric derived from the Linearized stratospheric ozone chemistry (Linoz; Mclinden et al., 2000; Hsu and Prather, 2009). The SSO assumes a “steady state” of ozone chemistry in stratosphere and is calculated in absence of dynamics, thereby isolates the

Deleted: tropical

Deleted: , with impact on the circulation and greenhouse gases that extends from the tropical stratosphere into the troposphere

Deleted: ¶

Deleted: In the lower stratosphere where the ozone chemistry is slow, t

Deleted: in the middle and upper stratosphere,

Deleted: ozone chemistry is fast and a chemical steady-state is maintained in spite of the transport. In this upper region the changes in vertical transport of trace gases like the total reactive nitrogen reservoir NO_y and the QBO dynamics-driven changes in temperature may also alter the ozone chemistry and produce new steady state values. ¶

Deleted: for attributing ozone variability and

Deleted: differences

Deleted: response

Deleted: and climate

Formatted: Font: 12 pt, Font color: Auto

Formatted: Font: 12 pt, Font color: Auto

Formatted: Subscript

Deleted: For example, the impact of the ozone depleting substances may be underestimated if chemistry-driven ozone is mis-interpreted as transport-driven ozone, leading to potential bias in ozone projection and associated radiation calculation. However

Deleted: dependence

Deleted: temperature

Deleted: Richter

Deleted: phase

117 impacts due to chemical reactions and temperature perturbations. The determination of transport-
 118 driven ozone is then based on the difference of modeled ozone from the steady-state ozone.
 119 Studies have shown the validity of using linearized chemistry for representing ozone (McLinden
 120 et al., 2020) and ozone response to 4xCO₂ (Meraner 2020), and our study build on it. The current
 121 state-of-art earth system model still have problem in simulating a realistic QBO. Until now, only
 122 15 of the 30 models in the Coupled Model Intercomparison Project phase 6 (CMIP6) have an
 123 internally generated QBO (Richter et al., 2020). Within these models, the simulated QBO
 124 amplitude and periods often fail to match the observed pattern. The World Climate Research
 125 Project (WCRP) Atmospheric Processes And their Role in Climate (APARC) started an QBO
 126 initiative (QBOi) in 2015 to improve Chemistry-Climate Model (CCM) simulation of tropical
 127 variability (Butchart et al., 2018). The phase II of QBOi includes a set of nudging experiments to
 128 examine QBO impact on climate, and here we build on those experiments.

129 In this study, we use the newly developed SSO metric on experiments following QBOi phase
 130 II protocol to disentangle the chemical and transport impact of QBO on ozone. Our primary
 131 modeling tool is the Department of Energy (DOE) Energy Exascale Earth Model version 2
 132 (E3SMv2, Golaz et al., 2022) with interactive stratospheric ozone (Linoz v2 and Linoz v3;
 133 McLinden et al., 2000; Hsu and Prather, 2009), and secondarily we examine some QBOi
 134 experiments from the National Center for Atmospheric Research (NCAR) Community Earth
 135 System Model (CESM). We also develop a new index of the QBO phase from a nonlinear
 136 principal component analysis (NLPCA) of the tropical zonal winds that better retains asymmetric
 137 patterns of QBO than standard linear PCA QBO index (Wallace et al., 1993). The phase-based
 138 composite diagrams are then created to investigate the temporal evolution of ozone patterns, both
 139 observed and modeled. We show that the SSO is a novel and effective tool in separating the
 140 chemical and transport process of QBO on ozone, and may be applied to diagnose the model-to-
 141 model discrepancy in QBO-ozone response. The observational data and ozone modeling are
 142 described in Sect. 2. The NLPCA method is presented in Sect. 3, followed by the description of
 143 the SSO in Sect. 4. The results are in Sect. 5. The discussion and conclusion are in Sect. 6.

144 2. Data and methods

145 2.1 CCM models

146 The primary model for this study is E3SMv2. E3SM's atmospheric component (EAMv2) is
 147 run here as a CCM with specified sea surface temperatures (SSTs) and has 72 vertical layers and

Moved (insertion) [3]

Deleted: E3SM

Deleted: ¶

Formatted: Subscript

Formatted: Font: (Default) Times New Roman, Font color: Auto

Deleted: The number of models with a naturally generated free-running QBO was 0 in the third Coupled Model Intercomparison Project (CMIP3); it rose to 5 in CMIP5 and to 15 in CMIP6 (Richter et al., 2020). Still,

Deleted: in these models

Deleted: In the current Chemistry–Climate Model Initiative (CCMI), many CCMs forced a QBO signal by nudging the equatorial zonal wind (Morgenstern et al., 2017). Nudging of the winds is inherently unphysical and produces an anomalous BDC not found in the free-running versions of the same CCMs (Orbe et al., 2020).

Deleted: the

Formatted: Indent: First line: 0"

Moved up [3]: The determination of transport-driven ozone is then based on the difference of E3SM modeled ozone from the steady-state ozone.

Deleted: interactive stratospheric chemistry module in E3SM (Linoz: McLinden et al., 2000; Hsu and Prather, 2009) as an off-line model to calculate the photochemical steady-state value of ozone in response the local chemical composition, the temperature and the overhead column of ozone that determine photolysis rates. The Linoz code is based on tabulated linearization of the net chemical production of ozone and thus steady-state ozone can be derived from linear algebra. The determination of transport-driven ozone is then based on the difference of E3SM modeled ozone from the steady-state ozone.

Deleted:

Deleted: Compared with the standard linear PCA QBO index (Wallace et al., 1993), NLPCA retains the observ... [1]

Deleted: ¶ ... [2]

Deleted: section

Deleted: s

Deleted: ion

Deleted: and use of the

Deleted: Linoz off-line chemistry model

Deleted: s

Deleted: ion

Deleted: s

Deleted: ion

Deleted: s

Deleted: ion

208 a horizontal resolution of about 100 km. Following Richter et al. (2010), EAMv2 employs
 209 gravity wave (GW) parameterizations that include orographic GWs (McFarlane, 1987),
 210 convective GWs (Beres et al., 2004), and GWs generated by frontal systems (Charron and
 211 Manzini, 2002). Tunable parameters in the orographic and frontal GW parameterizations remain
 212 the same as in EAMv1 (Xie et al., 2018; Rasch et al., 2019). The tunable parameters in
 213 convective GWs were explored to produce a more realistic QBO in EAMv2 with a period around
 214 27 months, much closer to observations (28 months) as compared to 16 months in EAMv1
 215 (Richter et al., 2019). Nevertheless, the modeled QBO remains weak in amplitude. Stratospheric
 216 ozone in E3SMv2 is calculated interactively through transport and the chemical Linoz module
 217 (McLinden et al., 2000; Hsu and Prather, 2009) that was updated from the E3SM O3v1 to O3v2
 218 module (Tang et al., 2021). Linoz v2 data tables are used to calculate the 24-hour-average ozone
 219 tendency (i.e., net production minus loss) from an adopted climatological mean state for key
 220 species (CH₄, H₂O, and NO_y, Cly, Bry) and first-order Taylor series expansions ~~of~~ the local
 221 ozone, temperature, and overhead ozone column (see Eq. (3) in Sect. 4.1). The data tables are
 222 generated for each year assuming key chemical species and families (CH₄, H₂O, and NO_y, Cly,
 223 Bry) follow monthly zonal-mean climatologies that scale with the slowly varying changes in
 224 tropospheric mean abundance of their source gases (e.g., N₂O, CFCs, halons, CH₄, tropopause
 225 H₂O). The Linoz model produces a reasonable stratospheric ozone climatology, including
 226 seasonal and interannual variability and the Antarctic ozone hole (Tang et al., 2021; Ruiz and
 227 Prather, 2022). The tropospheric chemical package for E3SMv2 (chemUCI) was not used and
 228 the lower boundary for Linoz was set to 30 ppb. Thus, none of the ozone column variability
 229 arises from tropospheric ozone chemistry. E3SMv2 diagnostics on the tendency of tropospheric
 230 ozone calculate a geographically resolved stratosphere-troposphere exchange (STE) flux of
 231 ozone every time step (Hsu et al., 2005; Tang et al., 2013).

Deleted: about

232 The secondary model for this study is CESM2 (Emmons et al., 2020), using a modified
 233 version of the community atmosphere model (CAM) with 83 vertical levels (Randall et al., 2023;
 234 Isla et al., 2024), which is run here as a CCM with specified sea surface temperatures (SSTs).
 235 CAM uses the finite-volume dynamical core with a nominal 1° horizontal resolution and with
 236 physics from the Whole Atmosphere Community Climate Model version 6 (WACCM6;
 237 Gettleman et al. 2019). The parameters for the convective GW momentum transport ~~scheme is~~
 238 tuned especially for this version to obtain a realistic, naturally generated QBO (Randall et al.,

Deleted: were

2023). The inline ozone calculation in CESM2 is replaced with a monthly mean 3D ozone climatology specified from a previous WACCM simulation. This input ozone forcing is formed by merging WACCM simulations for historical (1850-2014, 3 members) and future period (2015-2100, 1 member). As the mean of free-running CCM simulations, this ozone input climatology does not have any significant QBO-like variability, and thus it cannot trigger a QBO in the CCM (Butchart et al., 2023).

Both models are run with tropical winds being nudged to the observations and hence the synchronicity of the QBO should be similar and we can compare directly with observations. With the CESM2 QBO simulation we must limit our analysis to examining the forced dynamical response (temperature, circulation), but with E3SM results we can compare the modeled QBO-ozone interactions with observations.

2.2 Observed/reanalysis ozone and wind

For ozone, we derive the QBO signal from the monthly zonal mean total column ozone (TCO) using the Multi-Sensor Reanalysis version 2 data (MSRv2, R.J. van der A, et al. 2015). This latitude-by-month dataset initially covers the period 1979-2012 and later extended to 2020. For stratospheric profiles, we use the zonal monthly mean latitude-by-altitude from the Concentration Monthly Zonal Mean (CMZM) product (Sofieva et al., 2023). This altitude-by-month profile data covers the period 1985-2020. The vertical levels are converted to pressure levels inverting the pressure-altitude formula, $z^* = 16 \log_{10}(1000/P)$ km. We compared this ozone data with the overlapping period from the Microwave Limb Sounder (MLS) data (V5 Level 3: Schwartz et al., 2021) and found only small differences with regard to QBO patterns.

We use ERA5 data (wind, temperature, geopotential height) from the reanalysis produced by the European Center for Medium-Range Weather Forecast (ECMWF) Integrated Forecast System (Hersbach et al., 2020). The version we use has 137 hybrid sigma model levels from the surface to the model top at 0.01 hPa, and the horizontal resolution is about 31 km. We use monthly mean data for the period 1979–2020 to analyze the QBO-related dynamical changes, and 6-hourly ERA5 tropical zonal wind (15°N-15°S) to nudge model simulations mentioned below. We use the 5°S-5°N tropical average zonal wind from ERA5 and simulations to determinate the QBO phase index. The combined station zonal wind data from Freie University of Berlin (Naujokat, 1986) for the period of 1979-2020 is also used.

2.3 The QBOi simulations

Deleted: observed

We use two experiments from the protocol for phase-2 of the QBOi (Butchart et al., 2018; Bushell et al., 2020; Richter et al., 2020):

(1) Exp1-ObsQBO (nudged): the zonal wind in the tropical stratosphere is constrained to follow the observed QBO evolution by nudging it toward ERA5 reanalysis (Hitchcock et al. 2022). Thus, the stratospheric climate including temperature and circulation in the tropics is constrained.

(2) Exp1-AMIP (natural): the zonal wind in the tropical stratosphere evolves freely in each CCM being forced only by SSTs and trace-gas radiative forcing; there is no nudging. The SSTs are historical and include interannual variability, primarily El-Nino and Southern Oscillation (ENSO).

The nudging is applied to the zonal wind over the range 8 hPa-to-80 hPa and 15°S-to-15°N (Fig. S1, nudging coefficient shown is for E3SMv2, that for CESM2 is similar). There is a slight difference in how the models were nudged: E3SMv2 is nudged to the “full field” ERA5 wind field including the longitudinal variability, while CESM2 is nudged to the zonally-averaged ERA5 zonal wind field. The nudging relaxation timescale is 5 days. The current setup forces the models to match the tropical QBO dynamic variability while allowing other variabilities to evolve freely (e.g. semi-annual oscillation). For each experiment we produced 3 ensemble members, and the ensemble mean is used for analysis.

To better understand the QBO-chemistry interactions, we performed two additional nudged single-ensemble 1979-2020 runs with E3SMv2 using different chemical models: one with an expanded stratospheric chemistry Linoz-v3 (Hsu and Prather, 2010), which calculates NO_y-N₂O-CH₄-H₂O as prognostic tracers and includes their interactions with ozone; a second with fixed ozone climatology as prescribed for CESM2.

3. NLPCA analysis of QBO phase

To build a time-line composite picture of the QBO in any variable, we need to define a phase of each QBO, and align these phases over a 28-month period. Phase asymmetry and nonlinear features of the evolution of the QBO phase are found in many studies (Lindzen and Holton 1968; Holton and Lindzen, 1972; Giorgetta et al., 2002). The most obvious and sharply defined synchronization point is when the QBO west phase (QBOW, i.e. prevailing westerlies) transitions to the east phase (QBOe: prevailing easterlies) at some pressure level in the middle stratosphere (taken as 10 hPa here) (Naujokat et al., 1986; Pahlavan et al., 2021; Kang et al., 2022). The

Deleted: s

QBOe phase is typically longer (e.g., Bushell et al., 2019) with wind speeds about twice as strong as that of the QBOw (Naujokat et al., 1986; Kang et al., 2022). The problem with defining the QBO phase (index) simply as the month-to-month difference relative to the synchronization point (e.g., Ruiz et al., 2021) is that the duration of different phases varies across successive QBOs.

Previous use of PCA-derived QBO indices (Wallace et al., 1993) did not allow for this asymmetric and nonlinear behavior. Lu et al. (2009) noted that the reconstructed wind series from the PCA looked more sinusoidal in time than the actual winds, and thus the asymmetries between phases did not show up in the PCA-based indices. To address these issues, we use an NLPCA method that utilizes hierarchical-type neural network with an auto-associative architecture (Scholz et al. 2002). It is a nonlinear generalization of the standard PCA from straight lines to curves in the original data space, and natural extension to the PCA method by enforcing the nonlinear components to the same hierarchical order as in the standard PCA (Scholz et al., 2002). The NLPCA model described here has 5 layers with 3 hidden layers of neurons. The layers of the neural-network for NLPCA are in the sequence of input-encoding-bottleneck-decoding-output with the structure of $n-(2k+2)-k-(2k+2)-n$, where the n refers to dimension of input/output dataset and k is the number of dimensions for bottleneck layer. To achieve robustness, the NLPCA is applied to the tropical zonal wind data (5°S - 5°N , 10-hPa to 70-hPa) for a set of k varying from 2 to 5, with 100 runs (different in random initialization weights) for each k . The optimal number of k is set as 5 as it gives the lowest root-mean-square-error between the input and output. The comparison of QBO phase angles and QBO transition points are shown in Fig. S2a and S2b. It is shown that the first and second principal components (PC1 and PC2) of the NLPCA account for approximately 90% of the whole variance (Figs. S2c and S2d).

Following previous studies (Wallace et al., 1993; Hamilton and Hsieh, 2002; Lu et al., 2009), the QBO phase index ψ is calculated using PC1 and PC2 as follows:

$$\psi = \arctan(v/u) \quad (-\pi \leq \psi \leq \pi), \quad (1)$$

where u and v are the time series of the PC1 and PC2, respectively. The positive/negative phase angle index ψ corresponds to QBOw/QBOe.

We compare the reconstructed zonal wind anomalies using NLPCA and PCA (Wallace et al., 1993) with the QBO cycle in the observation (Fig. 1). It is shown that the observed QBO

transition corresponds to an abrupt downward propagation in QBOw and a slower downward transition in QBOe (indicated by clustering points in B to C to A on black triangular shape in Fig. 1a). The NLPCA captures large part of this sharp transition in QBOw while PCA underestimates it (indicated by points near C in Fig. 1a). This difference is also clearly shown in a typical QBO cycle of 1970. ~~September~~– 1972. ~~March~~ (Figs. 1b, 1c, and 1d, black arrow-sticks exhibits the downward propagation in QBOw) and the time series of NLPCA/PCA QBO phase (index) (Fig. S2).

NLPCA-derived QBO index is more realistic in following the atmospheric changes, it is impractical to map the NLPCA phases onto the monthly-mean model diagnostics. Thus, our QBO composites use simple monthly time steps about our best synchronization point, which from the NLPCA analysis we take to be at the transition when phase angle index ψ crosses 0 with negative values before and positive values after it (from QBO easterly to QBO westerly phase). It is demonstrated that comparing to QBO composites produced using the PCA-derived QBO index, those that produced using the NLPCA-derived index show a shifted QBO synchronization month (Fig. S2b). This results in larger contrast in observed tropical zonal wind anomalies between QBOw/QBOe (Figs. S3a and S3b) that is consistent with those described in previous literatures (Hamilton and Hsieh, 2002; Lu et al., 2009). This larger contrast between NLPCA and PCA in zonal wind anomalies is correspondent with the larger contrast in that of the total column ozone anomalies (Figs. S3c and S3d).

4. Linoz calculation of the steady-state ozone

To examine the ~~chemical~~ ozone response to the QBO we use ~~the SSO calculated from~~ both Linoz v2 and v3 models. ~~For Linoz-v2, this metric calculates local SSO response of ozone to the modeled changes in temperature, chemical species, and overhead ozone column; for Linoz-v3, more long-lived species are added.~~ For Linoz v2 the ~~SSO~~ is derived from Eq. 4 of McLinden et al. (2000). The photochemical ~~SSQ~~ mole fraction f_{ss} (parts per million, moles per mole of dry air) is expressed as follows:

$$f^{ss} = f^o + [(P - L)^o + \frac{\partial(P-L)}{\partial T}|^o (T - T^o) + \frac{\partial(P-L)}{\partial C_{O_3}}|^o (C_{O_3} - C_{O_3}^o)] \tau, \quad (2)$$

This is derived by setting $\frac{d(P-L)}{dt} = 0$ for Eq. 1 in McLinden et al., (2000). The values f^o , T^o , and $C_{O_3}^o$ are the climatological values of local ozone, temperature, and overhead column ozone tables used to calculate the Linoz tendencies. $(P-L)_o$ is the ozone net production minus loss

Deleted: 9

Deleted: 3

Deleted: While the

Deleted:

Deleted: steady-state ozone

Deleted: steady-state ozone

tendency and the partial derivatives are the sensitivity of the net production to temperature and overhead column ozone.

A major assumption of Linoz v2 here is that the key chemical families (NO_y , Cl_y , Br_y) and long-lived reactive gases (N_2O , CH_4 , H_2O) do not change from their climatological values used to generate the tables (Hsu and Prather, 2009). This steady-state calculation ignores transport tendencies and thus will be apply only where the photochemistry is rapid, i.e., $\tau =$

$-\left[\frac{\partial(P-L)}{\partial f}\right]_o^{-1} < 100$ days. Fig. 2 shows this Linoz v2 steady-state calculation (f_{ss} , T , τ) for January and July using ERA5 monthly mean temperature.

An alternative version (Linoz v3) of the **SSO** derived from Hsu and Prather (2010) is expressed as follows:

$$f_{ss} = f_o + [(P - L)_o + \frac{\partial(P-L)}{\partial T}|_o (T - T_o) + \frac{\partial(P-L)}{\partial C_{O_3}}|_o (C_{O_3} - C_{O_3}^o) + \sum_{j=1}^{j=5} \frac{\partial(P-L)}{\partial f_j}|_o (f_j - f_j^o)] \tau, \quad (3)$$

This is similar as [Eq. 2](#), except adds the contribution from sources of $f_{\text{N}_2\text{O}}$, f_{NO_y} , f_{CH_4} , $f_{\text{H}_2\text{O}}$. This may be used to provide a more precise diagnosis of the SSO from those models that have these output of chemistry species in addition to the temperature profile.

5. Impact of QBO on circulation and stratospheric ozone

Nudging the tropical zonal wind creates QBO-driven perturbations to the temperature and residual circulation that we can diagnose in both the E3SMv2 and CESM2 runs and compare with observations. For E3SMv2 with interactive ozone we are able to see the changes in ozone. This also applies to the simulations with an internally generated QBO.

We create a similar composite of the QBO cycle using E3SMv2/CESM2 following Ruiz et al., (2021) to see the full QBO cycle influence on stratospheric ozone. The time-composite is created for each month starting 14 months prior and extending to 14 months after the QBO transition for 1979-2020. The center **of the composite** is when the NLPCA-derived QBO phase angle index (see [Sect. 3](#)) shifts from negative to positive (QBOe -> QBOw). We create composites for circulation (zonal wind, temperature and residual circulation) and chemistry tracers (total column ozone (TCO), ozone concentration, NO_y) as a function of QBO phase. For TCO, we calculate the zonal-mean averages to produce the global map of composite; for all other fields, we process the tropical (15°S - 15°N) and extratropical (30°S - 60°S / 30°N - 60°N) vertical profile of regional average using latitudinal weight to produce the composites. The CESM2 ozone composite is not shown since its ozone is prescribed.

Deleted: steady state ozone

Deleted: equation

Deleted: s

Deleted: ion

406 The structure for this section is as follows; we first analyze the impact of nudged QBO on
 407 circulation in E3SM and CESM in Sect. 5.1, we then analyze its impact on global TCO and
 408 tropical/extratropical ozone in Sect. 5.2 and 5.3. The chemistry and transport impact of QBO are
 409 further analyzed using the SSO metric in Sect. 5.4. The overall performances of the models are
 410 summarized in Sect. 5.5.

411 5.1 Impact of QBO on circulation

412 In this section, we examine the impact of nudged QBO on circulation in both E3SMv2 and
 413 CESM2. We first analyze its impact on zonal wind and subsequently on temperature and residual
 414 circulation (e.g. \bar{w}^* , which characterizes the transport impact of the Brewer-Dobson Circulation).

415 Through nudging, the anomalous tropical zonal wind (15°S-15°N) in both nudged E3SMv2
 416 and CESM2 simulations exhibit a similar negative-positive-negative pattern to that of ERA5
 417 from QBOe to QBOw (Fig. 3). In terms of the magnitude, E3SMv2 zonal wind's pattern above
 418 6-hPa is minorly stronger than that of ERA5 and CESM2. Despite this minor difference, both
 419 models overall reproduce the QBO signal in the tropical nudging regions. Correspondent to the
 420 zonal wind changes shown in Fig. 3, the tropical temperature (Figs. 4a-c) in both models exhibit
 421 a negative-positive-negative-positive pattern like that of ERA5. Alongside is the residual vertical
 422 transport \bar{w}^* that exhibits a positive-negative-positive-negative pattern, like that of ERA5 (Figs.
 423 4d-f). Studies have documented the QBOe tends to relate to cooling and upward advection while
 424 QBOw relates to warming and downward advection (Baldwin et al., 2001). The tropical
 425 temperature and \bar{w}^* results shown are thus in-phase with zonal wind change in both models.

426 In the extratropic region (30°N-60°N/30°S-60°S), the results for the zonal wind are noisier
 427 (Fig. S4). The ERA5 results exhibit scattered signals of zonal wind changes for both hemispheres
 428 (Fig. S4a). The two models exhibit noisy results like that of ERA5, with CESM2 closer to ERA5.
 429 This is expected since the extratropics are more likely to be affected by dynamic noise from the
 430 polar regions. Unlike that of the zonal wind, the temperature and residual vertical transport \bar{w}^*
 431 results are smoother for both observation and nudged simulations. It is shown that ERA5 exhibits
 432 about two cycles of positive-negative phase change for temperature (Fig. 5a and 5d) and
 433 negative-positive phase change for \bar{w}^* (Figs. 6a and 6d) from QBOe to QBOw, although
 434 southern hemisphere (SH) is noisier than northern hemisphere (NH). Both models seem to have
 435 better agreement with ERA5 in the NH (Figs. 5b, 5c and Figs. 6b, 6c), while E3SMv2 performs
 436 better than CESM2 in the SH (Figs. 5e, 5f and Figs. 6e, 6f). Studies have documented that the

Deleted: In the following sections,

Deleted: section

Deleted: .

Deleted: W

Deleted: s

Deleted: ion

Deleted: steady-state ozone

Deleted: s

Deleted: ion

Deleted: s

Deleted: ion

Deleted: Figure

Deleted: 's

Deleted: positive-negative

Deleted: tropics

Deleted: (Figs. 4a-c)

Deleted: Figure

Deleted: accordance

Deleted: northern hemisphere

Deleted: southern hemisphere

457 QBO signal in the ~~extratropical~~ temperature and vertical advection are at about 180° phase
 458 change relative to the tropical QBO signal (Baldwin et al., 2001). The results shown here ~~are~~ in-
 459 phase with our nudged QBO signal in the tropics. Overall, the two models show some signals of
 460 QBO-related signals outside of the regions of nudging on temperature and \underline{w}^* , exhibiting the
 461 “spill-over” effect of QBO nudging.

462 To sum up, nudging creates ~~a~~ more realistic QBO signal in both E3SMv2 and CESM2
 463 especially in the tropical region. Outside of the nudging region, the “spill-over” effect of the
 464 nudged QBO is seen mostly on temperature and \underline{w}^* but less on the noisier zonal wind.

465 5.2 Impact of QBO on global TCO

466 In this section, we examine the impact of QBO on ozone using TCO ~~reanalysis~~ (MSRv2) and
 467 E3SMv2 model simulations. The TCO composites from the E3SMv2 nudged simulation is
 468 compared in Fig. 7. It is shown that the anomalous MSRv2 TCO exhibits a significant shift of
 469 tripole pattern from QBOe to QBOw (Fig. 7a). The ~~MSRv2~~ exhibits tri-pole pattern of
 470 anomalous low ~~TCO~~ in the tropics and high ~~TCO~~ in the extratropics during QBOe that gradually
 471 transits to tri-pole pattern of anomalous high ~~TCO~~ in the tropics and low ~~TCO~~ in the extratropic
 472 during QBOw. The magnitude of the ~~low~~ ~~TCO~~ in QBOe (5 DU) is lower than the positive
 473 pattern (12 DU) in QBOw in the tropics, indicating asymmetric phase response of TCO to QBO
 474 in the tropics. The E3SMv2 nudged simulation is like MSRv2 in that it captures most of the
 475 tripole patterns in both phases with similar amplitudes (Fig. 7b), indicating the impact of nudged
 476 QBO on TCO is close to what observed. It is shown that the internally generated QBO variability
 477 in E3SMv2 natural (Fig. S5a) only partly exhibits the patterns of MSRv2 with weaker amplitude
 478 (nearly eight times weaker). ~~Since the response of column ozone is mainly driven by the wind in~~
 479 ~~the lower stratosphere, this discrepancy likely indicates that the internal generated QBO is too~~
 480 ~~weak there. This and the good result in nudging run (Fig. 7b) indicate that nudging the tropical~~
 481 ~~zonal wind contributes to the modulation and enhancement of this “QBO-driven” TCO~~
 482 ~~variability in E3SMv2.~~

483 Overall, the nudged E3SMv2 simulations show “QBO-driven” TCO variability in accordance
 484 to observation that is partly present in E3SMv2 natural simulations and enhanced by QBO
 485 nudging.

486 5.3 Impact of QBO on tropical/extratropical stratospheric ozone

Deleted: extratropics

Deleted: is

Deleted: observations

Deleted: TCO pattern

Deleted: negative

Moved down [1]: This indicates that nudging the tropical zonal wind contributes to the modulation and enhancement of this “QBO-driven” TCO variability in E3SMv2.

Deleted: This indicates that nudging the tropical zonal wind contributes to the modulation and enhancement of this “QBO-driven” TCO variability in E3SMv2.

Moved (insertion) [1]

Deleted: s

Deleted: ¶

500 In this section, we analyze the impact of QBO on tropical (15°S-15°N) and extratropical
 501 (30°S-60°S/30°N-60°N) stratospheric ozone concentration. The composites of ozone vertical
 502 profile (1-hPa to 100-hPa) from E3SMv2 nudged and E3SMv2 Linoz-v3 nudged simulations are
 503 compared with the CMZM satellite data (Fig. 8).

504 In the tropics, it is shown that the CMZM satellite ozone exhibits a double-peak vertical
 505 structure with large ozone variations between 1~20-hPa and 20~100-hPa (Fig. 8a). Both peaks
 506 shift in a sequence of negative-positive-negative from QBOe to QBOw, and the amplitude of the
 507 upper peak is smaller than that of the lower peak (Fig. 8a). The E3SMv2 nudged simulation
 508 captures most of the double-peak structure (Fig. 8b) with minor exceptions – the anomalous high
 509 ozone in CMZM from month -14 to month -8 around 10-hPa and the anomalous low around 10-
 510 hPa from month -2 to month 2 is missed. Studies have documented NO_y variations as the
 511 primary drivers of ozone QBO changes around this range (Chipperfield et al., 1994; Tian et al.,
 512 2006). Since nudged E3SMv2 simulation uses the Linoz-v2 which the chemical species such as
 513 CH₄ or NO_y remain constant, the deficiency may be due to uncertainty in these chemical species.
 514 To test this assumption, we also compared the E3SMv2 Linoz-v3 nudged simulation (with
 515 chemistry of NO_y-N₂O-CH₄-H₂O included) with CMZM (Fig. 8c). It is shown that the E3SMv2
 516 Linoz-v3 nudged simulation captures both missing ozone fluctuation between 6-hPa to 10-hPa in
 517 E3SMv2 nudged, indicating that this missing chemistry may be responsible for this deficiency.
 518 The E3SMv2 natural simulations, on the other hand, show similar double-peaked patterns but
 519 with smaller amplitude (3 times weaker) and shorter period (Fig. S5b). This may be because the
 520 period of internally generated QBO in E3SMv2 is ~21 years (Golaz et al., 2022). Overall, the
 521 E3SMv2 nudged simulation modifies the period and enhances the QBO response in tropical
 522 ozone that is mostly consistent with the CMZM weaker above 20-hPa and stronger below 20-
 523 hPa.

524 This analysis is extended to the E3SMv2 nudged simulations in the extratropical region in
 525 both hemispheres (30°N-60°N/30°S-60°S). Since the nudging is imposed only in the tropical
 526 regions, we can further examine the impact of nudged QBO in the extratropics where it is free
 527 running. Fig. 9 shows pressure-time cross-section of the extratropical (30°N-60°N/30°S-60°S)
 528 ozone concentration as a function of QBO phase for CMZM satellite ozone, E3SMv2 nudged
 529 and E3SMv2 Linoz-v3 nudged simulations. Unlike that of the tropics, the extratropical ozone for
 530 CMZM is noisier despite an overall in-phase change with QBO (Figs. 9a and 9d). The exception

Deleted: s

Deleted: nudged

Deleted: stry

Deleted: chemistry

Deleted: impact

Deleted: Figure

Deleted: parts

Deleted: with deficiency around 10-hPa. This deficiency is rectified by improved representation of NO_y-N₂O-CH₄-H₂O chemistry in E3SMv2 Linoz-v3 nudged simulation

is in the **NH** where the QBOw exhibits an extra phase change to positive (Fig. 9a). It is shown that nudged E3SMv2 simulations follow the similar positive-negative ozone phase shift in both hemispheres (Figs. 9b and 9e) without the noisy phase changes in the **NH**. In terms of the amplitude, the QBOw is similar for both hemispheres but being weaker than CMZM in QBOe. The ozone change in the E3SMv2 Linoz-v3 nudged simulation tends to be similar to that of the E3SMv2 nudged simulation, except the amplitude in QBOw is stronger (Figs. 9c and 9f). Overall, the E3SMv2 nudged and E3SMv2 Linoz-v3 nudged partly capture in-shift with QBO in extratropical ozone in both hemispheres despite amplitude difference.

5.4 Separating the chemistry and transport impact of QBO on ozone using steady-state ozone

In this section, we utilize the **SSO** (Eq. 2 and 3, see Sect. 4 for detail) introduced in Sect. 4 to separate the chemistry and transport impact of QBO on ozone. As a coupled system, the QBO chemical and transport impacts on ozone are intertwined, making it difficult to diagnose which QBO impact is more prominent to the ozone differences between model and observation or among different models. Here we try to quantitatively separate these two terms with this new diagnostic tool, recognizing their time scale differences. We first derive the Linoz-v2 **SSO** (Eq. 2) for E3SMv2 nudged and CESM2 nudged simulations (Fig. 10). Although ozone is prescribed in CESM2, the **SSO** for CESM2 shown here is the temperature-ozone impact due to the CESM2 temperature profiles. To further analyze impact of temperature and different chemistry species (NO_y , N_2O , H_2O , CH_4) in ozone simulation, the **SSO** using temperature only (Eq. 2) and using temperature plus chemistry species (Eq. 3) are derived for E3SMv2 Linoz-v3 nudged (Fig. 11).

In the tropics (15°S - 15°N), the Linoz-v2 **SSO** from E3SMv2 and CESM2 nudged exhibit an apparent negative-positive-negative pattern above 20-hPa (Figs. 10a and 10d). These corresponds to the temperature patterns above 20-hPa shown in the previous section (Figs. 4b and 4c). This pattern in E3SMv2 is like that of the E3SMv2 ozone pattern above 20-hPa (Fig. 8b), indicating a temperature impact mostly above 20-hPa. Below 20-hPa, the prognostic ozone in E3SMv2 correspond to the alternating w^* shift patterns (Fig. 4e). The residual meridional circulation shows a weaker magnitude below 20-hPa and is thus less likely to play a major role in ozone change (Fig. S6). This and the lack of response in **SSO** indicates the prognostic ozone below 20-hPa in E3SMv2 is transport-driven. Like that of the analysis in the tropics, the temperature impact in the extratropics (30°N - 60°N / 30°S - 60°S) is stronger above 20-hPa for both

Deleted: northern hemisphere

Deleted: northern hemisphere

Deleted: Linoz

Deleted: Linoz

Deleted: steady-state ozone

Deleted: equation

Deleted: s

Deleted: ion

Deleted: s

Deleted: ion

Deleted: steady state ozone

Deleted: equation

Deleted: steady state ozone

Deleted: the "would-be"

Deleted:

Deleted: if CESM2 were to implement Linoz v2 as its ozone module...

Deleted: the

Deleted: steady state ozone

Deleted: equation

Deleted: equation

Deleted: steady state ozone

Deleted: no

Deleted: steady state ozone

596 E3SMv2 (Figs. 10b and 10c) and CESM2 (Figs. 10e and 10f) nudged simulations. The
 597 difference is that temperature in the SH (30°S-60°S) is overall noisier than that of the northern
 598 hemisphere (30°N-60°N). This noisier SH SSO above 20-hPa in the nudged simulations
 599 correspond to the noisier temperature for the two models (Figs. 5c and 5f), which may be largely
 600 affected by stronger and noisier southern polar vortex (Fig. S7) as also documented by other
 601 studies (Ribera et al., 2004). The intrusion of the polar vortex via event like sudden stratospheric
 602 warming (Butler et al., 2017) may have an impact on the QBO-ozone relationship in the
 603 extratropics. Below 20-hPa, the E3SMv2 nudged ozone corresponds to the w* (Fig. 10b and
 604 10c), indicating it's transport-driven. Overall, with the application of Linoz-v2 on E3SMv2
 605 nudged simulation, we can partly separate the temperature-driven and transport-driven QBO-
 606 ozone around the boundary of 20-hPa in both tropics and extratropics. The limit in this
 607 application lies in the uncertainty in exclusion of chemistry transport such as NO_y in the
 608 simulations.

609 To test the sensitivity of the results to the chemistry variations, we further applied Linoz-v2
 610 SSO (Eq. 2, temperature-only) and Linoz-v3 SSO (Eq. 3, temperature plus chemistry) to
 611 E3SMv2 Linoz-v3 nudged simulation (Fig. 11). It is shown that the SSO including temperature
 612 plus chemistry variation show better accordance with MSRv2 ozone (Figs. 8a, 9a, 9d) than
 613 including temperature only especially in both the tropics (Figs. 11a, and 11d) and the extratropics
 614 (Figs. 11c, 11d, 11e, and 11f). This better accordance is especially apparent between 6-hPa to 20-
 615 hPa and in good accordance with the NO_y change (Fig. 12), indicating the impact of chemistry
 616 variation within this height. To further examine the variable responsible for the change, we also
 617 did the single specie sensitivity test (not shown). It is shown that including temperature plus NO_y
 618 variation can reproduce the patterns in Figs. 11a-c. This indicates the NO_y variation an important
 619 driver around 6-hPa to 20-hPa in QBO-ozone, in accordance with the previous studies
 620 (Chipperfield et al., 1994; Tian et al., 2006).

621 The results here indicate demarcations of QBO-induced ozone at 6-hPa and 20-hPa. These
 622 demarcations of the QBO-induced ozone at 6-hPa and 20-hPa may be due to the separation of
 623 ozone lifetime below/above 20-hPa (Reed et al., 1964) and NO_y variation (Chipperfield et al.,
 624 1994; Tian et al., 2006). The ozone lifetime is relatively long compared with the dynamical
 625 process below 20-hPa while shortened considerably above it. The temperature affects ozone
 626 above 20-hPa (especially above 6-hPa) through ozone destruction – warmer anomalies accelerate

Deleted: Southern Hemisphere

Deleted: southern hemisphere

Deleted: steady state ozone

Deleted: s

Deleted: sudden

Deleted: steady-state ozone

Deleted: equation

Deleted: steady-state ozone

Deleted: equation

Deleted: steady-state ozone

Deleted: observed

Deleted: 8a,

Deleted: 9a, 9b,

Deleted: is also done

Deleted: this level

Deleted: colder/

Deleted: slow/

644 ozone destruction, leading to correspondent ozone decrease (Wang et al., 2022), *vice versa*; the
 645 transport effect of QBO-related wind modulates the temperature through thermal wind balance
 646 enhancing/lessening the upward motion in the tropics (Plumb and Bell, 1982; Baldwin et al.,
 647 2001; Ribera et al., 2004; Punge et al., 2009). In the extratropics, the process is similar except
 648 *that is* controlled by the return *branch* of QBO-induced circulation that is in 180° phase reversal
 649 with the tropics (Baldwin et al., 2001). This explains the apparent separation of transport- and
 650 chemistry-driven ozone changes above/below 20-hPa. Between 6-hPa to 20-hPa, QBO
 651 modulation of NO_y variation is shown to be an important contributor of the QBO-ozone cycle in
 652 addition to the temperature impact (Chipperfield et al., 1994). This explains the better
 653 reproduction of *SSQ* above 20-hPa when including NO_y variation. *Ozone transport, on the other*
 654 *hand, plays a relatively weaker role above 20-hPa.* Overall, the demarcations of QBO-induced
 655 ozone shown here can be overall explained by photochemical process above 6-hPa, NO_y
 656 variation between 6-hPa and 20-hPa, and circulation change in vertical advection below 20-hPa.
 657 It is also worth mentioning that the nudged CESM2 also produces similar temperature and *w**
 658 *patterns*. This indicates that nudged CESM2 may produce similar prognostic ozone if *Linoz were*
 659 *to be implemented* as interactive ozone module.

Deleted: increase/

Deleted: arm

Deleted: steady

Deleted: -state ozone

Deleted: it were to implement Linoz

660 5.5 Model performance in simulating QBO impact

661 In this sub-section, we examine the overall performance of E3SMv2 and CESM2 QBOi
 662 simulations in simulating the QBO-ozone relationship. We evaluate the pattern correlation and
 663 standard deviation of the area-weighted TCO pattern (60°S-60°N), vertically-weighted ozone
 664 concentration (15°S-15°N, 30°N-60°N, 30°S-60°S), zonal wind (15°S-15°N, 30°N-60°N, 30°S-
 665 60°S), temperature (15°S-15°N, 30°N-60°N, 30°S-60°S), and *w** (15°S-15°N, 30°N-60°N, 30°S-
 666 60°S). For ozone, only E3SMv2 results are shown since CESM2 has fixed ozone. The results are
 667 summarized in a Taylor diagram shown in Fig. 13. The observed pattern is plotted at the (1,0)
 668 reference point.

669 In terms of ozone (Fig. 13a), there are remarkable differences between the simulations.
 670 Overall, the E3SMv2 nudged simulations perform the best, with the pattern correlation of all
 671 four variables over 0.8 while other simulations are below 0.5. This indicates nudging realistic
 672 QBO variability may increase the model performance in simulating ozone. In the extratropics,
 673 the E3SMv2 nudged simulation has good pattern correlations, but the amplitude is off by over

679 1.5 times. The results for temperature, zonal wind and w^* are similar with ozone in the tropics
 680 (Figs. 13b, 13c, and 13d). What's different is in the extratropics — both nudged
 681 E3SMv2/CESM2 temperature, zonal wind, and w^* show better performance in NH extratropics
 682 than in SH extratropics. This may be due to stronger polar vortices in SH and NH that disturb the
 683 QBO signal (Ribera et al., 2004). Another difference is in the natural simulations – the tropical
 684 temperature (15°S-15°N) and zonal wind signals exhibit reasonable correlations of over 0.7 in
 685 zonal wind, over 0.5 in temperature. This indicates a discernable internally generated QBO
 686 signal in the E3SMv2/CESM2, although it's weaker and does not extend to the extratropics.

687 6. Discussion and conclusion

688 6.1 Discussion

689 There are some interesting issues worth discussing in this section. First, the use of the SSO
 690 provides an useful tool to diagnose the dynamical and chemical impact of the QBO on ozone. The
 691 Linoz v2 SSO metric can be applied to all models with the minimum need of temperature profile
 692 only. One caveat of this approach is that Linoz-v2 SSO neglects the potential impact of cross-over
 693 chemical species such as the NO_y as in SSO that has been shown to be an important driver for
 694 QBO-ozone change between 6-hPa to 20-hPa. Thus, it would be recommended to include at least
 695 the NO_y output by the CCMs and include it in SSO calculation (Eq. 3) for a more precise diagnostic
 696 between this height range. The QUasi-Biennial oscillation and Ozone Chemistry interactions in
 697 the Atmosphere (QUOCA) proposed a new joint QBOi-CCMI project to improve understanding
 698 of the QBO-ozone feedback in present-day and future climates. The tools shown here may be
 699 useful to diagnose the uncertainty in QBO-ozone relationship among different model simulations
 700 in this project.

701 Another noteworthy issue is the nudging employed in the current study. Nudging has been
 702 adopted by models from different climate centers in the QBOi project to ensure the realistic
 703 simulation of QBO through constraining the tropical climate. The different strategies of nudging
 704 in these models and their effects on the QBO climate are thus needed to be analyzed with care.
 705 Our study showed that the nudging overall constrains both E3SMv2 and CESM2 towards a
 706 realistic representation of QBO-associated temperature and residual circulation field outside of the
 707 nudged regions (15°S-15°N tropics). However, differences in the nudging strategies can play a
 708 role in the detailed features of the zonal wind and temperature simulated by the two models. For

Deleted: C

Deleted: ly

Deleted: offline Linoz model

Deleted: with the

Deleted: current

Moved down [4]: The tools shown here can be valuable to diagnose the uncertainty in the QBO-ozone relationship among difference models.

Moved (insertion) [4]

Deleted: can

Deleted: valuable

Deleted: the

Deleted: ce

Deleted: s

Deleted: ¶

Deleted: differences in the

example, the extratropical zonal wind and temperature in CESM2 showed more scattered features than those in E3SMv2 in our simulations. This may be partly because the full field nudging in E3SMv2 nudge all zonal wavenumbers. This may pose a stronger constraint on field than the zonal mean nudging in CESM2 that may nudge less spectrum of zonal wavenumbers.

Deleted: field of high

Thirdly, our study shows the importance of including $\text{NO}_y\text{-N}_2\text{O-CH}_4\text{-H}_2\text{O}$ chemistry in the linearized ozone representation of climate model. Our study shows that the E3SMv2 Linoz v2 simulation with linearized ozone may underestimate the QBO-ozone amplitude above 10-hPa, as also documented in Meraner et al., (2020). The E3SMv2 Linoz-v3 simulation with $\text{NO}_y\text{-N}_2\text{O-CH}_4\text{-H}_2\text{O}$ chemistry, on the other hand, improves this QBO-ozone magnitude especially between 6-hPa to 10-hPa. Meraner et al., (2020) demonstrated the usefulness of linearized ozone in representing ozone due to negligible computational cost, despite its deficiency in simulating QBO-ozone magnitude. The inclusion of $\text{NO}_y\text{-N}_2\text{O-CH}_4\text{-H}_2\text{O}$ chemistry may contribute to alleviating this issue.

Deleted:

Deleted: ly

Deleted: with

Last, the impact of ozone feedback on the climate in this study deems further attention. The two models compared here show overall similar QBO-signal over the nudging runs despite have two different ozone modules – one interactive and another non-interactive. One may question what the results would be with the same modules under nudging. The sensitivity test of E3SMv2 fixed-ozone nudged simulation shows that with fixed-ozone, the temperature patterns are still retained although with an amplified magnitude in both the tropics and extratropics (Fig. S8). This indicates a strong nudging impact, and an overall damping effect of interactive ozone in E3SMv2.

Deleted: S7

6.2 Conclusion

In this study, we utilize the SSO on nudged climate model simulations to separate the chemical and transport response of the QBO ozone impact. We derive a new QBO phase index using the NLPCA method and utilize this index to form QBO cycle composites to analyze QBO-ozone relationships in observation and simulations. By analyzing the simulations from two QBOi participant models (E3SMv2 and CESM2), we found that the nudged simulations can produce a reasonable QBO impact in the tropics and create “spill-over” impact to the extratropical fields like temperature and residual circulation. The nudged E3SMv2 simulation captures the tripole composite pattern in the observed TCO. Nudging was also shown to improve the double-peaked vertical structure in observed ozone data between 1~20-hPa and 20~100-hPa over the tropics. In the extratropics outside of the nudging region, the nudged E3SMv2 simulated ozone tends to be

Deleted: Linoz

Deleted: steady state ozone

Deleted: on

Deleted: in the extratropics to be in-phase with tropic QBO signal

overall in-phase with the observed but with magnitude difference, indicating the “spill-over” impact of nudged QBO signal.

Utilizing the *SSO* metric, we separated the chemical and transport response of ozone in E3SMv2 nudged to QBO. It is shown that these impacts have rather clear demarcations on both tropical and extratropical ozone response at 6-hPa and 20-hPa – chemistry impact correspondent to QBO-related temperature changes dominates the response above 6-hPa linked to photochemical processes and between 6-hPa to 20-hPa linked to NO_y variation, and transport impact related to QBO-related vertical advection dominates the response below 20-hPa. The results here are important for diagnosing model-model and model-observation differences in the QBO with free-running climate simulations, allowing us to separate chemical from circulation effects.

Stratospheric ozone is not only essential for protecting life on the Earth but also has important climate impacts. More and more studies reported the important role of ozone variations in modifying the stratospheric circulation and therefore influencing the surface climate (e.g. Xie et al., 2020). Since the QBO has relatively high predictability, considering its impacts on stratospheric ozone and subsequent atmospheric circulations may help improve the predictions of surface weather and climate (e.g., Li et al., 2023).

Despite the above studies, however, there are still caveats. The current study makes use of only one model in QBOi that has an interactive ozone feature. More models may be used in the future to examine the QBO-ozone relationship. These are to be assessed in future studies.

Data availability

The satellite data from the Copernicus Climate Change Service can be accessed at (<https://cds.climate.copernicus.eu/cdsapp#!/dataset/satellite-ozone-v1?tab=form>). The ERA5 data can be accessed at (<https://cds.climate.copernicus.eu/cdsapp#!/dataset/reanalysis-era5-complete?tab=overview>). The ChemDyg diagnostics can be accessed at (<https://doi.org/10.5281/zenodo.11166488>).

Author contribution

J.X., Q.T. designed the research; J.X. performed the E3SM simulations and wrote the manuscript. J.R. provided the CESM2 simulation. Q. T. and M.P.’s supervised the research and

Deleted: Linoz steady-state ozone

Deleted: ,

Deleted: -change

helped interpreting the results. All authors contributed to the scientific discussion and paper revision.

Competing interests

The authors declare that they have no conflict of interest.

Acknowledgement

We thank the Copernicus Climate Change Service for providing the satellite data and ECMWF for the ERA5 data. We thank Isla Simpson for setting up the CESM2 QBOi simulations, and providing the Python script for generating the Transformed Eulerian Mean variables. We thank Sasha Glenville for transferring the CESM2 data. This research was supported as part of the E3SM project, funded by the U.S. Department of Energy, Office of Science, Office of Biological and Environmental Research. Part of the work was supported by the LLNL LDRD project 22-ERD-008 titled “Multiscale Wildfire Simulation Framework and Remote Sensing”. E3SM simulations were performed on a high-performance computing cluster provided by the BER ESM program and operated by the Laboratory Computing Resource Center at Argonne National Laboratory. Additional post-processing and data archiving of production simulations used resources of the National Energy Research Scientific Computing Center (NERSC), a DOE Office of Science User Facility supported by the Office of Science of the U.S. Department of Energy under Contract No. DE-AC02-05CH11231. This work was performed under the auspices of the U.S. Department of Energy by Lawrence Livermore National Laboratory under contract DE-AC52-07NA27344. The IM release number is LLNL-JRNL-858987. This work was in part supported by the National Center for Atmospheric Research (NCAR), which is a major facility sponsored by the National Science Foundation (NSF) under Cooperative Agreement 1852977. Portions of this study were supported by the Regional and Global Model Analysis (RGMA) component of the Earth and Environmental System Modeling Program of the U.S. Department of Energy’s Office of Biological and Environmental Research (BER) via NSF Interagency Agreement 1844590.

Reference

- Andrews, M. B., Knight, J. R., Scaife, A. A., et al.: Observed and Simulated Teleconnections Between the Stratospheric Quasi-Biennial Oscillation and Northern Hemisphere Winter Atmospheric Circulation, *J. Geophys. Res.*, 124, 1219–1232, <https://doi.org/10.1029/2018JD029368>, 2019.
- Andrews, D.G., J.R. Holton, and C.B. Leovy: *Middle Atmosphere Dynamics*. Academic Press, 489pp, 1987.
- Anstey, J. A. and Shepherd, T. G.: High-latitude influence of the quasi-biennial oscillation, *Q. J. Roy. Meteor. Soc.*, 140, 1–21, <https://doi.org/10.1002/qj.2132>, 2014.
- Baldwin, M. P., Birner, T., Brasseur, G., et al.: 100 years of progress in understanding the stratosphere and mesosphere, *Meteor. Mon.*, 59, 27.1–27.62, <https://doi.org/10.1175/AMSMONOGRAPHSD-19-0003.1>, 2019.
- Baldwin, M. P., Gray, L. J., Dunkerton, T. J., et al.: The quasi-biennial oscillation, *Rev. Geophys.*, 39, 179–229, 2001.
- Baldwin M. P., Tung K.K., Extra-tropical QBO signals in angular momentum and wave forcing. *Geophys. Res. Lett.* 21: 2717–2720, 1994.
- Beljaars, A. C. M., Brown, A. R., & Wood, N.: A new parameterization of turbulent orographic form drag. *Quarterly Journal of the Royal Meteorological Society*, 130, 1327–1347. <https://doi.org/10.1256/qj.03.73>, 2004.
- Bowman, K. P.: Global patterns of the quasi-biennial oscillation in total ozone. *J. Atmos. Sci.*, 46, 3382–3343, 1989.
- Brasseur, G., Hauglustaine, D., Walters, S., Rasch, P., Muller, J., Granier, C., & Tie, X.: MOZART, a global chemical transport model for ozone and related chemical tracers 1. Model description. *Journal of Geophysical Research-Atmospheres*, 103(D21), 28,265–28,289. <https://doi.org/10.1029/98JD02397>, 1998.
- Burkholder, J. B., Sander, S. P., Abbatt, J., Barker, J. R., Huie, R. E., Kolb, C. E., et al.: Chemical kinetics and photochemical data for use in atmospheric studies, evaluation no. 18, JPL Publication 15–10, Jet Propulsion Laboratory, Pasadena, CA. Retrieved from <http://jpldataeval.jpl.nasa.gov>, 2015.
- Bushell, A. C., Anstey, J. A., Butchart, N., et al.: Evaluation of the quasi-biennial oscillation in global climate models for the SPARC QBO-initiative. *Quarterly Journal of the Royal Meteorological Society*, 148(744), 1459–1489, 2020.
- Butchart, N., Andrews, M. B., & Jones, C. D.: QBO phase synchronization in CMIP6 historical simulations attributed to ozone forcing. *Geophysical Research Letters*, 50, e2023GL104401. <https://doi.org/10.1029/2023GL104401>, 2023.
- Butchart, N., Anstey, J. A., Hamilton, K., et al.: Overview of experiment design and comparison of models participating in phase 1 of the SPARC Quasi-Biennial Oscillation initiative (QBOi). *Geoscientific Model Development*, 11(3), 1009–1032, 2018.
- Butchart, N., Charlton-Perez, A. J., Cionni, I., et al.: Multimodel climate and variability of the stratosphere, *J. Geophys. Res.*, 116, D05102, <https://doi.org/10.1029/2010JD014995>, 2011.
- Butchart, N., Scaife, A.A., Austin, J., et al.: Quasi-biennial oscillation in ozone in a coupled chemistry-climate model. *J. Geophys. Res.: Atmosphere* 108 (D15), 4486, 2003.
- Butler, A. H., Sjöberg, J. P., Seidel, D. J., Rosenlof, K. H.: A sudden stratospheric warming compendium, *Earth System Science Data*. 9 (1): 63–76. doi:10.5194/essd-9-63-2017.

870 Charron, M., and Manzini, E.: Gravity waves from fronts: Parameterization and middle
871 atmosphere response in a general circulation model. *Journal of the Atmospheric Sciences*,
872 59(5), 923–941. [https://doi.org/10.1175/1520-0469\(2002\)059<0923:gwffpa>2.0.co;2](https://doi.org/10.1175/1520-0469(2002)059<0923:gwffpa>2.0.co;2), 2002.
873 Chipperfield, M. P., & Gray, L. J.: Two-dimensional model studies of the interannual
874 variability of trace gases in the middle atmosphere. *Journal of Geophysical Research:*
875 *Atmospheres*, 97(D5), 5963–5980, 1992.
876 [Chipperfield, M., Bekki, S., Dhomse, S. et al.: Detecting recovery of the stratospheric ozone](#)
877 [layer. *Nature* 549, 211–218, 2017. <https://doi.org/10.1038/nature23681>](#)
878 Chipperfield, M. P., Gray, L. J., Kinnarsley, J. S., Zawodny, J.: A two-dimensional model study
879 of the QBO signal in SAGE II NO₂ and O₃. *Geophysical research letters*, 21(7), 589–592,
880 1994.
881 Coy, L., Wargan, K., Molod, A. M., et al.: Structure and dynamics of the quasi-biennial
882 oscillation in MERRA-2, *J. Climate*, 29, 5339–5354, 2016.
883 Danabasoglu, G., Lamarque, J.-F., Bacmeister, J. et al.: The Community Earth System Model
884 Version 2 (CESM2). *Journal of Advances in Modeling Earth Systems*, 12, e2019MS001916.
885 <https://doi.org/10.1029/2019MS001916>, 2020.
886 Dunkerton, T. J.: The role of gravity waves in the quasi-biennial oscillation, *J. Geophys. Res.*,
887 102, 26,053–26,076, 1997.
888 Elsbury, D., Peings, Y., and Magnusdottir, G.: Variation in the Holton-Tan effect by longitude,
889 *Q. J. Roy. Meteor. Soc.*, 147, 1767–1787, <https://doi.org/10.1002/qj.3993>, 2021.
890 Emmons, L. K., Schwantes, R. H., Orlando, J. J., et al.: The Chemistry Mechanism in the
891 Community Earth System Model version 2 (CESM2). *Journal of Advances in Modeling Earth*
892 *Systems*, 12, e2019MS001882. <https://doi.org/10.1029/2019MS001882>, 2020.
893 Emmons, L. K., Hauglustaine, D. A., Müller, J. F., Carroll, M. A., Brasseur, G. P., Brunner, D.,
894 et al.: Data composites of airborne observations of tropospheric ozone and its precursors.
895 *Journal of Geophysical Research-Atmospheres*, 105(D16), 20497–20538.
896 <https://doi.org/10.1029/2000jd900232>, 2000.
897 Garfinkel, C. I., Shaw, T. A., Hartmann, D. L., and Waugh, D. W.: Does the Holton-Tan
898 Mechanism Explain How the Quasi-Biennial Oscillation Modulates the Arctic Polar Vortex?, *J.*
899 *Atmos. Sci.*, 69, 1713–1733, <https://doi.org/10.1175/JAS-D-11-0209.1>, 2012.
900 Gettelman, A., & Morrison, H.: Advanced two-moment bulk microphysics for global models.
901 Part I: Off-line tests and comparison with other schemes. *Journal of Climate*, 28, 1268–1287.
902 <https://doi.org/10.1175/JCLI-D-14-00102.1>, 2015.
903 Giorgetta, M. A., Manzini, E., and Roeckner, E.: Forcing of the quasi-biennial oscillation from
904 a broad spectrum of atmospheric waves. *Geophysical Research Letters*, 29(8), 86-1, 2002.
905 Golaz, J.-C., Van Roekel, L. P., Zheng, X. et al.: The DOE E3SM Model version 2: Overview
906 of the physical model and initial model evaluation. *Journal of Advances in Modeling Earth*
907 *Systems*, 14, e2022MS003156. <https://doi.org/10.1029/2022MS003156>, 2022.
908 Golaz, J.-C., Caldwell, P. M., Van Roekel, L. P. et al.: The DOE E3SM coupled model version
909 1: Overview and evaluation at standard resolution. *Journal of Advances in Modeling Earth*
910 *Systems*, 11(7), 2089–2129. <https://doi.org/10.1029/2018MS001603>, 2019.
911 Golaz, J.-C., Larson, V. E., & Cotton, W. R. A PDF-based model for boundary layer clouds.
912 Part I: Method and model description. *Journal of the Atmospheric Sciences*, 59, 3540–3551,
913 2002.
914 Gray, L. J., & Dunkerton, T. J.: The role of the seasonal cycle in the quasi-biennial oscillation
915 of ozone. *Journal of Atmospheric Sciences*, 47(20), 2429–2452, 1990.

Formatted: Font: (Default) Times New Roman, Font color: Auto, Pattern: Clear

Formatted: Font: (Default) Times New Roman, Font color: Auto, Pattern: Clear

Formatted: Font: (Default) Times New Roman, Font color: Auto, Pattern: Clear

Formatted: Font: (Default) Times New Roman, Font color: Auto, Pattern: Clear

916 Hamilton, K., & Hsieh, W. W.: Representation of the quasi-biennial oscillation in the tropical
 917 stratospheric wind by nonlinear principal component analysis. *Journal of Geophysical*
 918 *Research: Atmospheres*, 107(D15), ACL-3, 2002.
 919 Hamilton, K. : Interhemispheric asymmetry and annual synchronization of the ozone quasi-
 920 biennial oscillation. *Journal of Atmospheric Sciences*, 46(7), 1019-1025, 1989.
 921 Hansen, F., Matthes, K., and Gray, L. J.: Sensitivity of stratospheric dynamics and chemistry to
 922 QBO nudging width in the chemistryclimate model WACCM, *J. Geophys. Res.*, 118, 10464–
 923 10474, <https://doi.org/10.1002/jgrd.50812>, 2013.
 924 Hasebe, F.: Quasi-biennial oscillations of ozone and diabatic circulation in the equatorial
 925 stratosphere, *J. Atmos. Sci.*, 51, 729–745, 1994.
 926 Hersbach H, Bell B, Berrisford P, et al.: The ERA5 global reanalysis, *Q J R Meteorol Soc.*
 927 2020; 146: 1999–2049. <https://doi.org/10.1002/qj.3803>, 2020,
 928 Hitchcock, P., Butler, A., Charlton-Perez, A., et al.: Stratospheric Nudging And Predictable
 929 Surface Impacts (SNAPSI): a protocol for investigating the role of stratospheric polar vortex
 930 disturbances in subseasonal to seasonal forecasts. *Geoscientific Model Development*, 15(13),
 931 5073-5092, 2022.
 932 Hitchman, M. H., and C. B. Leovy: Estimation of the Kelvin wave contribution to the
 933 semiannual oscillation, *J. Atmos. Sci.*, 45, 1462, 1988.
 934 Holton, J. R. and Tan, H.-C.: The quasi-biennial oscillation in the Northern Hemisphere lower
 935 stratosphere, *J. Meteor. Soc. Japan.*, 60, 140–148, 1982.
 936 Holton, J. R. and Tan, H.-C.: The influence of the equatorial quasi-biennial oscillation on the
 937 global circulation at 50 mb, *J. Atmos. Sci.*, 37, 2200–2208, 1980.
 938 Holton, J. R.: Influence of the annual cycle in meridional transport on the quasi-biennial
 939 oscillation in total ozone. *Journal of Atmospheric Sciences*, 46(10), 1434-1439, 1989.
 940 Holton, J. R., and R. S. Lindzen: An updated theory for the quasi-biennial cycle of the tropical
 941 stratosphere, *J Atmos. Sci.*, 29, 1076, 1972.
 942 Horowitz, L. W., Walters, S., Mauzerall, D. L., Emmons, L. K., Rasch, P. J., Granier, C., et al.:
 943 A global simulation of tropospheric ozone and related tracers: Description and evaluation of
 944 MOZART, version 2. *Journal of Geophysical Research-Atmospheres*, 108(D24), 4784.
 945 <https://doi.org/10.1029/2002jd002853>, 2003.
 946 Hsu, J. and Prather, M. J.: Stratospheric variability and tropospheric ozone, *J. Geophys. Res.-*
 947 *Atmos.*, 114, D06102, <https://doi.org/10.1029/2008JD010942>, 2009.
 948 Hsu, J., and M. J. Prather: Global long-lived chemical modes excited in a 3-D chemistry
 949 transport model: Stratospheric N₂O, NO_y, O₃ and CH₄ chemistry, *Geophys. Res. Lett.*, 37,
 950 L07805, doi:[10.1029/2009GL042243](https://doi.org/10.1029/2009GL042243), 2010.
 951 Hsu, J., M. J. Prather, and O. Wild: Diagnosing the stratosphere-to-troposphere flux of ozone in
 952 a chemistry transport model, *J. Geophys. Res.*, 110, D19305, doi:[10.1029/2005JD006045](https://doi.org/10.1029/2005JD006045), 2005.
 953 Isla et al.: Toward the vertical resolution of the next generation of the Community Atmosphere
 954 Model, To be submitted, 2024.
 955 Jones, D. B., Schneider, H. R., & McElroy, M. B.: Effects of the quasi-biennial oscillation on
 956 the zonally averaged transport of tracers. *Journal of Geophysical Research: Atmospheres*,
 957 103(D10), 11235-11249, 1998.
 958 Jucker, M., Reichler, T., & Waugh, D. W.: How frequent are Antarctic sudden stratospheric
 959 warmings in present and future climate?. *Geophysical Research Letters*, 48(11),
 960 e2021GL093215, 2021.

961 Kang, M. J., Chun, H. Y., Son, S. W., et al.: Role of tropical lower stratosphere winds in quasi-
 962 biennial oscillation disruptions. *Science Advances*, 8(27), eabm7229, 2022.
 963 Kinnnersley, J. S., and Tung, K. K.: Mechanisms for the extratropical QBO in circulation and
 964 ozone. *Journal of the atmospheric sciences*, 56(12), 1942-1962, 1999.
 965 Kinnison, D. E., Brasseur, G. P., Walters, S., Garcia, R. R., Marsh, D. R., Sassi, F., et al.:
 966 Sensitivity of chemical tracers to meteorological parameters in the MOZART-3 chemical
 967 transport model. *Journal of Geophysical Research-Atmospheres*, 112(D20), D20302.
 968 <https://doi.org/10.1029/2006jd007879>, 2007.
 969 Lamarque, J. F., Emmons, L. K., Hess, P. G., Kinnison, D. E., Tilmes, S., Vitt, F., et al.: CAM-
 970 chem: Description and evaluation of interactive atmospheric chemistry in the Community Earth
 971 System Model. *Geoscientific Model Development*, 5(2), 369–411. [https://doi.org/10.5194/gmd-](https://doi.org/10.5194/gmd-5-369-2012)
 972 [5-369-2012](https://doi.org/10.5194/gmd-5-369-2012), 2012.
 973 Larson, V. E. : CLUBB-SILHS: A parameterization of subgrid variability in the atmosphere.
 974 arXiv:1711.03675v2 [physics.ao-ph], 2017.
 975 Lawrence, B. N. : A gravity-wave induced quasi-biennial oscillation in a three-dimensional
 976 mechanistic model. *Quarterly Journal of the Royal Meteorological Society*, 127(576), 2005-
 977 2021, 2001.
 978 Lee, S., Shelow, D., Thompson, A.M., Miller, S.: QBO and ENSO variability in temperature
 979 and ozone from SHADOZ, 1998–2005. *J. Geophys. Res.: Atmosphere* 115 (D18105), 2010.
 980 Lee, H.-H., Tang, Q., and Prather, M.: E3SM Chemistry Diagnostics Package (ChemDyg)
 981 Version 0.1.4, Geosci. Model Dev. Discuss. [preprint], <https://doi.org/10.5194/gmd-2023-203>,
 982 2024.
 983 Leung, L. R., Bader, D. C., Taylor, M. A., and McCoy, R. B.: An introduction to the E3SM
 984 special collection: Goals, science drivers, development, and analysis. *Journal of Advances in*
 985 *Modeling Earth Systems*, 12, e2019MS001821, 2020. <https://doi.org/10.1029/2019MS001821>
 986 Li, Y., Richter, J. H., Chen, C.-C., & Tang, Q.: A strengthened teleconnection of the quasi-
 987 biennial oscillation and tropical easterly jet in the past decades in E3SMv1. *Geophysical*
 988 *Research Letters*, 50, e2023GL104517. <https://doi.org/10.1029/2023GL104517>, 2023.
 989 Lin, S. J., & Rood, R. B.: An explicit Flux-Form Semi-Lagrangian shallow water model on the
 990 sphere. *Quarterly Journal of the Royal Meteorological Society*, 123, 2477–2498.
 991 Lindzen, R. S., and J. R. Holton (1968), A theory of the quasi-biennial oscillation, *J. Atmos.*
 992 *Sci.*, 25, 1095, 1997.
 993 Logan, J. A., M. J. Prather, S. C. Wofsy, and M. B. McElroy: Atmospheric Chemistry -
 994 Response to Human Influence. *Philos T R Soc A*, 290, 187-234, 1978.
 995 Lu, B. W., Pandolfo, L., and Hamilton, K.: Nonlinear representation of the quasi-biennial
 996 oscillation. *Journal of the atmospheric sciences*, 66(7), 1886-1904, 2009.
 997 Marquardt, C., & Naujokat, B.: An update of the equatorial QBO and its variability. *World*
 998 *Meteorological Organization-Publications-WMO TD, 1*, 87-90, 1997.
 999 Maycock, A. C., Randel, W. J., Steiner, A. K., Karpechko, A. Y., Christy, J., Saunders, R., et
 1000 al.: Revisiting the mystery of recent stratospheric temperature trends, 2018. *Geophysical*
 1001 *Research Letters*, 45, 9919–9933. <https://doi.org/10.1029/2018GL078035>
 1002 McFarlane, N. A.: The effect of orographically excited gravity wave drag on the general
 1003 circulation of the lower stratosphere and troposphere. *Journal of the Atmospheric Sciences*,
 1004 44(14), 1775– 1800. [https://doi.org/10.1175/1520-0469\(1987\)044<1775:teooeg>2.0.co;2](https://doi.org/10.1175/1520-0469(1987)044<1775:teooeg>2.0.co;2),
 1005 1987.

Deleted: , in review

McLinden, C. A., Olsen, S. C., Hannegan, B., et al.: Stratospheric ozone in 3-D models: A simple chemistry and the cross-tropopause flux, *J. Geophys. Res.*, 105(D11), 14653–14665, doi:10.1029/2000JD900124, 2000.

Mengel, J. G., H. G. Mayr, K. L. Chan, et al.: Equatorial oscillations in the middle atmosphere generated by small-scale gravity waves, *Geophys. Res. Lett.*, 22, 3027-3030, 1995.

Meraner, K., Rast, S., & Schmidt, H. (2020). How useful is a linear ozone parameterization for global climate modeling? *Journal of Advances in Modeling Earth Systems*, 12, e2019MS002003. <https://doi.org/10.1029/2019MS002003>

Morgenstern, O., Hegglin, M. I., Rozanov, E., et al.: Review of the global models used within phase 1 of the Chemistry–Climate Model Initiative (CCMI), *Geosci. Model Dev.*, 10, 639–671, <https://doi.org/10.5194/gmd-10-639-2017>, 2017.

Naujokat, B.: An update of the observed quasi-biennial oscillation of the stratospheric winds over the tropics. *J. Atmos. Sci.*, 43, 1873-1877, 1986.

Orbe, C., Plummer, D. A., Waugh, D. W., et al.: Description and Evaluation of the specified-dynamics experiment in the Chemistry–Climate Model Initiative, *Atmos. Chem. Phys.*, 20, 3809–3840, <https://doi.org/10.5194/acp-20-3809-2020>, 2020.

Park, M., and Coauthors: Variability of stratospheric reactive nitrogen and ozone related to the QBO. *J. Geophys. Res. Atmos.*, 122, 10 103–10 118, <https://doi.org/10.1002/2017JD027061>, 2017.

Pahlavan, H. A., Fu, Q., Wallace, J. M., & Kiladis, G. N.: Revisiting the quasi-biennial oscillation as seen in ERA5. Part I: Description and momentum budget. *Journal of the Atmospheric Sciences*, 78(3), 673-691, 2021a.

Pahlavan, H. A., Wallace, J. M., Fu, Q., & Kiladis, G. N.: Revisiting the quasi-biennial oscillation as seen in ERA5. Part II: Evaluation of waves and wave forcing. *Journal of the Atmospheric Sciences*, 78(3), 693-707, 2021b.

Park, M., Randel, W. J., Kinnison, D. E., et al.: Variability of stratospheric reactive nitrogen and ozone related to the QBO. *Journal of Geophysical Research: Atmospheres*, 122(18), 10-103, 2017.

Pawson, S., K. Labitzke, R. Lenschow, et al.: Climatology of the Northern Hemisphere stratosphere derived from Berlin analyses, part 1, Monthly means, technical report, Ser. A, 7(3), Freie Univ. Berlin, 1993.

PhotoComp: Chapter 6 - Stratospheric Chemistry SPARC Report No. 5 on the Evaluation of Chemistry–Climate Models 194-202, 2010.

Plumb, R. A., and R. C. Bell: A model of the quasi-biennial oscillation on an equatorial beta-plane, *Q. J. R. Meteorol. Soc.*, 108, 335-352, 1982.

Prather, J. M., Remsberg, E. E.: The Atmospheric Effects of Stratospheric Aircraft: Report of the 1992 Models and Measurements Workshop. (M.J. Prather, E.E. Remsberg, Eds.), Satellite Beach, FL, 144+268+352 pp, 1993.

Politowicz, P. A., & Hitchman, M. H.: Exploring the effects of forcing quasi-biennial oscillations in a two-dimensional model. *Journal of Geophysical Research: Atmospheres*, 102(D14), 16481-16497, 1997.

Randall, D. A., Tziperman, E., Branson, M. D., Richter, J. H., & Kang, W.: The QBO-MJO connection: A possible role for the SST and ENSO. *Journal of Climate*, 1-36, 2023.

Randel, W. J., & Cobb, J. B.: Coherent variations of monthly mean total ozone and lower stratospheric temperature. *Journal of Geophysical Research: Atmospheres*, 99(D3), 5433-5447, 1994.

Formatted: Default Paragraph Font, Font: (Default) Times New Roman, 12 pt, Font color: Auto, Pattern: Clear

Formatted: Default Paragraph Font, Font: (Default) Times New Roman, 12 pt, Font color: Auto, Pattern: Clear

1053 Randel, W. J., Wu, F., Russell, J. M., Roche, A., & Waters, J. W.: Seasonal cycles and QBO
 1054 variations in stratospheric CH₄ and H₂O observed in UARS HALOE data. *Journal of the*
 1055 *atmospheric sciences*, 55(2), 163-185, 1998.
 1056 Randel, W. J., and F. Wu: Isolation of the ozone QBO in SAGE II data by singular value
 1057 decomposition. *J. Atmos. Sci.*, **53**, 2546–2559, 1996.
 1058 Rasch, P. J., Xie, S., Ma, P.-L., et al.: An overview of the atmospheric component of the
 1059 Energy Exascale Earth System Model. *Journal of Advances in Modeling Earth Systems*, 11(8),
 1060 2377–2411. <https://doi.org/10.1029/2019ms001629>, 2019.
 1061 Reed, R.: A tentative model of the 26-month oscillation in tropical latitudes. *Q. J. R. Meteorol.*
 1062 *Soc.* 90, 441–466, 1964.
 1063 Richter, J. H., Anstey, J. A., Butchart, N., Kawatani, Y., Meehl, G. A., Osprey, S., & Simpson,
 1064 I. R.: Progress in simulating the quasi-biennial oscillation in CMIP models. *Journal*
 1065 *Geophysical Research: Atmospheres*, 125, e2019JD032362.
 1066 <https://doi.org/10.1029/2019JD032362>, 2020.
 1067 Richter, J. H., Chen, C.-C., Tang, Q., et al.: Improved simulation of the QBO in E3SMv1.
 1068 *Journal of Advances in Modeling Earth Systems*, 11(11), 3403–3418.
 1069 <https://doi.org/10.1029/2019MS001763>, 2019.
 1070 Ruiz, D. J., Prather, M. J., Strahan, S. E., et al.: How atmospheric chemistry and transport drive
 1071 surface variability of N₂O and CFC-11. *Journal of Geophysical Research: Atmospheres*, 126,
 1072 e2020JD033979. <https://doi.org/10.1029/2020JD033979>, (2021).
 1073 Ruiz, D. J. and M.J. Prather: From the middle stratosphere to the surface, using nitrous oxide to
 1074 constrain the stratosphere–troposphere exchange of ozone, *Atmos. Chem. Phys.*, 22, 2079–
 1075 2093, doi: 10.5194/acp-22-2079-2022, 2022.
 1076 Sander, et al. : Chemical kinetics and photochemical data for use in atmospheric studies,
 1077 evaluation number 15, in JPL Publication 06-2., Jet Propul. Lab., Pasadena, Calif., 2006.
 1078 Scaife, A. A., et al. (2014), Predictability of the quasi-biennial oscillation and its northern
 1079 winter teleconnection on seasonal to decadal timescales, *Geophys. Res. Lett.*, 41, 1752–1758,
 1080 doi:[10.1002/2013GL059160](https://doi.org/10.1002/2013GL059160).
 1081 Scholz M. and Vigário R.: Nonlinear PCA: a new hierarchical approach, *Proceedings of the*
 1082 *10th European Symposium on Artificial Neural Networks (ESANN)*, pp. 439-444., 2002.
 1083 Schwartz, M., Froidevaux, L., Livesey, N., Read, W., and Fuller, R.: MLS/Aura Level 3
 1084 Monthly Binned Ozone (O₃) Mixing Ratio on Assorted Grids V005, Greenbelt, MD, USA,
 1085 Goddard Earth Sciences Data and Information Services Center (GES DISC) [data set],
 1086 https://disc.gsfc.nasa.gov/datasets/ML3MBO3_005/summary (last access: 30 May 2024), 2021.
 1087 Scinocca, J., & McFarlane, N.: The parametrization of drag induced by stratified flow over
 1088 anisotropic orography. *Quarterly Journal of the Royal Meteorological Society*, 126, 2353–2394.
 1089 <https://doi.org/10.1256/smsqj.56801>, 2000.
 1090 Shibata, K.: Simulations of Ozone Feedback Effects on the Equatorial Quasi-Biennial
 1091 Oscillation with a Chemistry–Climate Model. *Climate*, (9), 123.
 1092 <https://doi.org/10.3390/cli9080123>, 2021.
 1093 Shuckburgh, E., Norton, W., Iwi, A., & Haynes, P.: Influence of the quasi-biennial oscillation
 1094 on isentropic transport and mixing in the tropics and subtropics. *Journal of Geophysical*
 1095 *Research: Atmospheres*, 106(D13), 14327-14337, 2001.
 1096 Sofieva, V. F., Szelag, M., Tamminen, J., et al.: Updated merged SAGE-CCI-OMPS+ dataset
 1097 for the evaluation of ozone trends in the stratosphere, *Atmos. Meas. Tech.*, 16, 1881–1899,
 1098 <https://doi.org/10.5194/amt-16-1881-2023>, 2023.

Formatted: Indent: Left: 0"

Stone, K.A., Solomon, S., Kinnison, D.E., On the identification of ozone recovery. *Geophys. Res. Lett.* 45, 5158–5165, 2018.

Tang, Q., Prather, M. J., Hsu, et al.: Evaluation of the interactive stratospheric ozone (O3v2) module in the E3SM version 1 Earth system model, *Geosci. Model Dev.*, 14, 1219–1236, <https://doi.org/10.5194/gmd-14-1219-2021>, 2021.

Tang, Q., Golaz, J.-C., Van Roekel, L. P.: The fully coupled regionally refined model of E3SM version 2: overview of the atmosphere, land, and river results, *Geosci. Model Dev.*, 16, 3953–3995, <https://doi.org/10.5194/gmd-16-3953-2023>, 2023.

Tang, Q., P. G. Hess, B. Brown-Steiner, and D. E. Kinnison : Tropospheric ozone decrease due to the Mount Pinatubo eruption: Reduced stratospheric influx, *Geophys. Res. Lett.*, 40, 5553–5558, doi:10.1002/2013GL056563, 2013.

Tian, W., Chipperfield, M.P., Gray, L.J., Zawodny, J.M.: Quasi-biennial oscillation and tracer distributions in a coupled chemistry-climate model. *J. Geophys. Res.: Atmosphere* 111 (D20), 2006.

Tilmes, S., Lamarque, J. F., Emmons, L. K., Kinnison, D. E., Ma, P. L., Liu, X., et al.: Description and evaluation of tropospheric chemistry and aerosols in the Community Earth System Model (CESM1.2). *Geoscientific Model Development*, 8(5), 1395–1426. <https://doi.org/10.5194/gmd-8-1395-2015>, 2015.

Tilmes, S., Lamarque, J. F., Emmons, L. K., Kinnison, D. E., Marsh, D., Garcia, R. R., et al.: Representation of the Community Earth System Model (CESM1) CAM4-chem within the Chemistry-Climate Model Initiative (CCMI). *Geoscientific Model Development*, 9(5), 1853–1890. <https://doi.org/10.5194/gmd-9-1853-2016>, 2016.

Tung, K. K., and H. Yang: Global QBO in circulation and ozone. Part I: Reexamination of observational evidence. *J. Atmos. Sci.*, 51, 2699–2707, 1994.

Tweedy, O. V., Kramarova, N. A., Strahan, S. E., et al., (2017), Response of trace gases to the disrupted 2015–2016 quasi-biennial oscillation, *Atmos. Chem. Phys.*, 17, 6813–6823, 2017.

van der A, R. J., Allaart, M. A. F., and Eskes, H. J.: Extended and refined multi sensor reanalysis of total ozone for the period 1970–2012, *Atmos. Meas. Tech.*, 8, 3021–3035, <https://doi.org/10.5194/amt-8-3021-2015>, 2015.

Wallace, J., Panetta, R., and Estberg, J.: Representation of the equatorial stratospheric quasibiennial oscillation in EOF phase space, *J. Atmos. Sci.*, 50, 1751–1762, [https://doi.org/10.1175/1520-0469\(1993\)050<1751:ROTESQ>2.0.CO;2](https://doi.org/10.1175/1520-0469(1993)050<1751:ROTESQ>2.0.CO;2), 1993.

Wang L., Hardiman, S. C., Bett, P. E. et al.: What chance of a sudden stratospheric warming in the southern hemisphere?. *Environmental Research Letters*, 15 (10): 104038. doi:10.1088/1748-9326/aba8c1. ISSN 1748-9326, 2020.

Wang, W., Hong, J., Shangguan, M., et al.: Zonally asymmetric influences of the quasi-biennial oscillation on stratospheric ozone. *Atmospheric Chemistry and Physics*, 22(20), 13695–13711, 2022.

Watson, P. A. G. and Gray, L. J.: How Does the Quasi-Biennial Oscillation Affect the Stratospheric Polar Vortex?, *J. Atmos. Sci.*, 71, 391–409, <https://doi.org/10.1175/JAS-D-13-096.1>, 2014.

Xie, F., Zhang, J., Li, X., et al.: Independent and joint influences of eastern Pacific El Niño–southern oscillation and quasi biennial oscillation on Northern Hemispheric stratospheric ozone, *Int. J. Climatol.*, 12, 5289–5307, <https://doi.org/10.1002/joc.6519>, 2020.

Formatted: Indent: Left: 0.1", First line: 0", Line spacing: single

1144 Xie, S., Lin, W., Rasch, P. J., et al.: Understanding cloud and convective characteristics in
 1145 version 1 of the E3SM Atmosphere Model. *Journal of Advances in Modeling Earth Systems*,
 1146 10(10), 2618–2644. <https://doi.org/10.1029/2018ms001350>, 2018.
 1147 Zhang, J., Xie, F., Ma, Z., et al.: Seasonal Evolution of the Quasibiennial Oscillation Impact on
 1148 the Northern Hemisphere Polar Vortex in Winter, *J. Geophys. Res.*, 124, 12568–12586,
 1149 <https://doi.org/10.1029/2019JD030966>, 2019.
 1150 Zhang, J., Xie, F., Ma, Z., Zhang, C., et al.: Seasonal Evolution of the Quasibiennial Oscillation
 1151 Impact on the Northern Hemisphere Polar Vortex in Winter, *J. Geophys. Res.*, 124, 12568–
 1152 12586, <https://doi.org/10.1029/2019JD030966>, 2019.
 1153 Zhang, R., Tian, W., and Wang, T.: Role of the quasi-biennial oscillation in the downward
 1154 extension of stratospheric northern annular mode anomalies, *Clim. Dynam.*, 55, 595–612, 2019.
 1155 Zhang, J., Chongyang Z., Kequan Z., et al.: The role of chemical processes in the quasi-
 1156 biennial oscillation (QBO) signal in stratospheric ozone. *Atmospheric Environment* 244,
 1157 117906, 2021.

Deleted: ¶

Formatted: Font: (Default) Times New Roman, 12 pt,
Font color: Auto, Pattern: Clear

Formatted: Font: (Default) Times New Roman, 12 pt,
Font color: Auto, Pattern: Clear

Formatted: Font: (Default) Times New Roman, 12 pt,
Font color: Auto, Pattern: Clear

Formatted: Font: (Default) Times New Roman, 12 pt,
Font color: Auto, Pattern: Clear

Formatted: Font: (Default) Times New Roman, 12 pt,
Font color: Auto, Pattern: Clear

Formatted: Font: (Default) Times New Roman, 12 pt,
Font color: Auto, Pattern: Clear

Formatted: Indent: Left: 0.1", Line spacing: single,
Border: Top: (No border), Bottom: (No border), Left: (No
border), Right: (No border), Between : (No border)

Formatted: Font: (Default) Times New Roman, 12 pt,
Font color: Auto, Pattern: Clear

Formatted: Font: (Default) Times New Roman, 12 pt,
Font color: Auto, Pattern: Clear

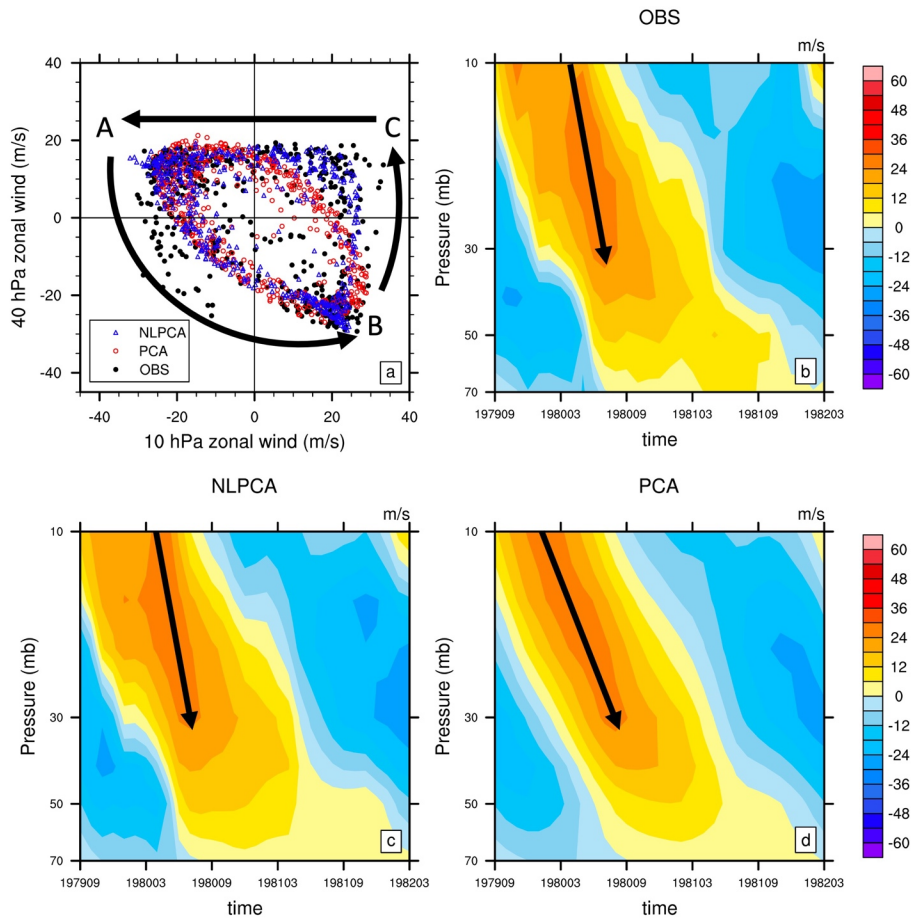


Figure 1 (a) Scatter-plot of 1979-2020 monthly mean zonal wind anomaly (m/s) at 10-hPa vs 40-hPa for observation (black), NLPCA reconstruction (blue), and PCA reconstruction (red). Typical cycle of QBO (1979 September-1982 March) from (b) Observational station data from University of Berlin, (c) NLPCA reconstruction, (d) PCA reconstruction.

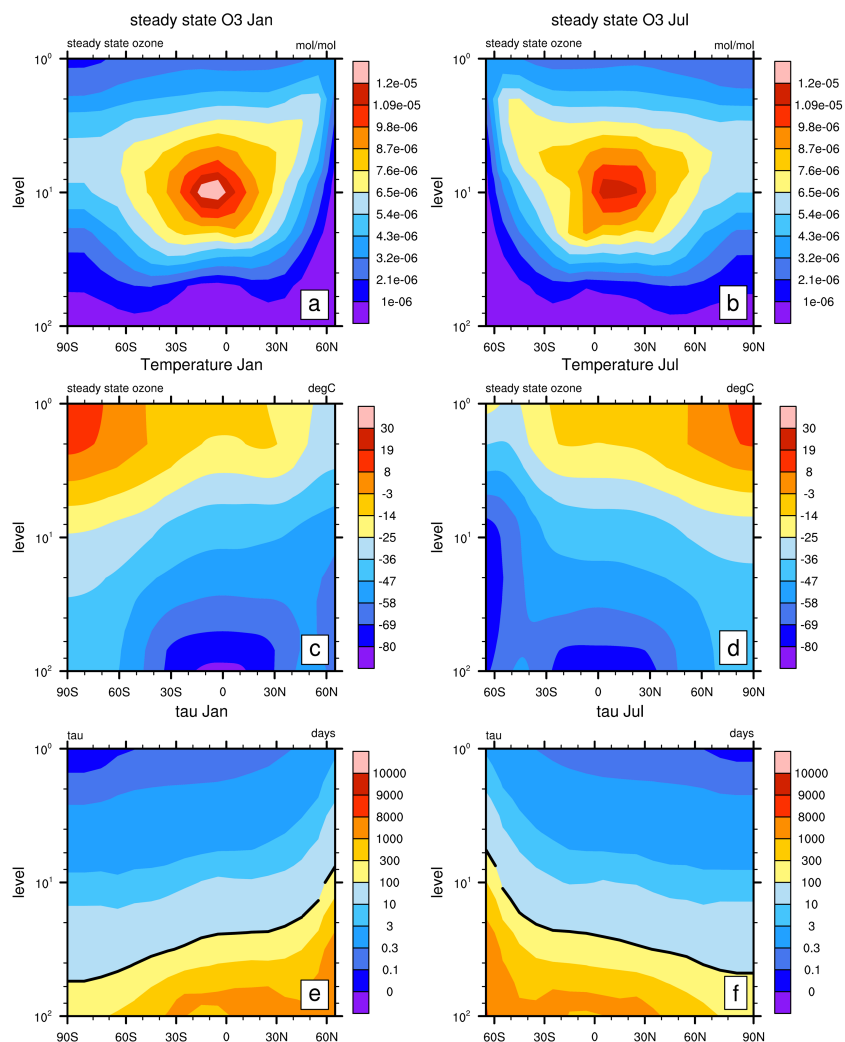
Deleted: .

Deleted: anomalous

Deleted:

Deleted: 09

Deleted: 03



1172

1173

1174

1175

1176

Figure 2 The (a, b) steady state ozone (mol/mol) derived using Linoz-v2 on E3SMv2 temperature, (c, d) ERA5 temperature (°C), (e, f) photochemical relaxation time τ (days), and for January and July. The thick black line in (c, d) denotes the 300 value-line.

Deleted: .

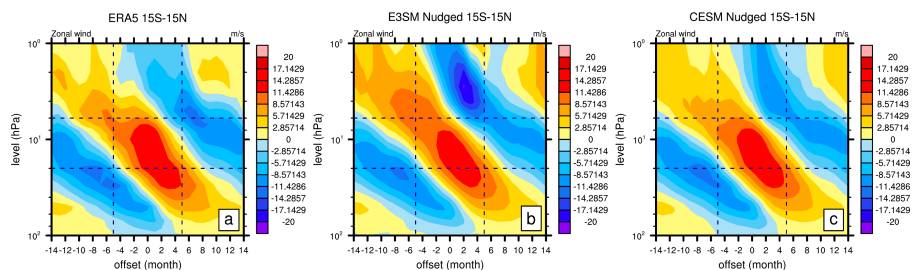


Figure 3 Pressure-time cross-section of the tropical (15°S-15°N) zonal wind anomaly (m/s) as function of QBO phase for (a, d) ERA5, (b, e) E3SMv2, (c, f) CESM2 for 1979-2020. 0 is centered on the month when QBO index shifts from QBOc to QBOw (determined by when current QBO index < 0 and next QBO index > 0). The QBO phase is determined by 5S-5N average of the zonal wind.

Deleted: .

Deleted: anomalous

Deleted:

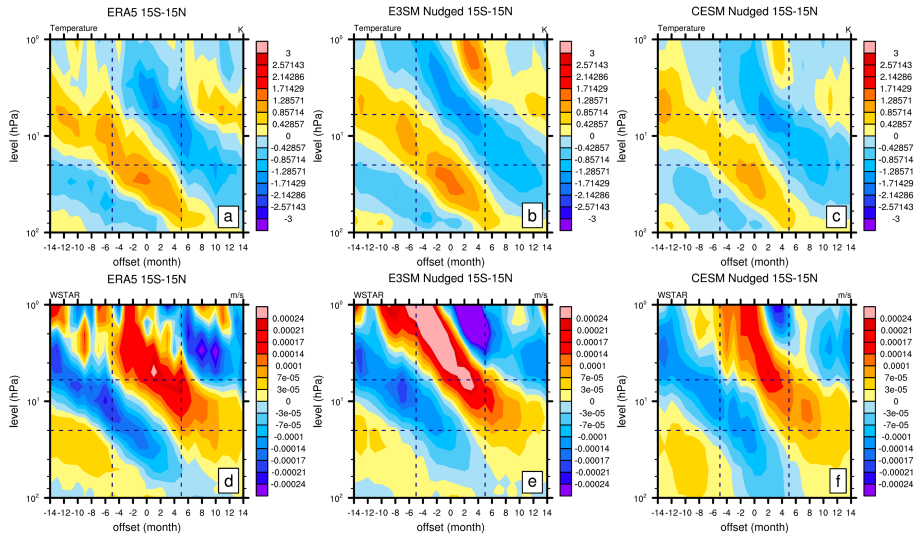


Figure 4 Pressure-time cross-section of the tropical (15°S-15°N) temperature (K) and w^* anomaly (Transformed Eulerian Mean residual vertical transport, m/s) as function of QBO phase for (a, d) ERA5, (b, e) E3SMv2, (c, f) CESM2 for 1979-2020. 0 is centered on the month when QBO index shifts from QBOe to QBOw (determined by when current QBO index < 0 and next QBO index > 0). The QBO phase is determined by 5S-5N average of the zonal wind.

Deleted: .

Deleted: anomalous

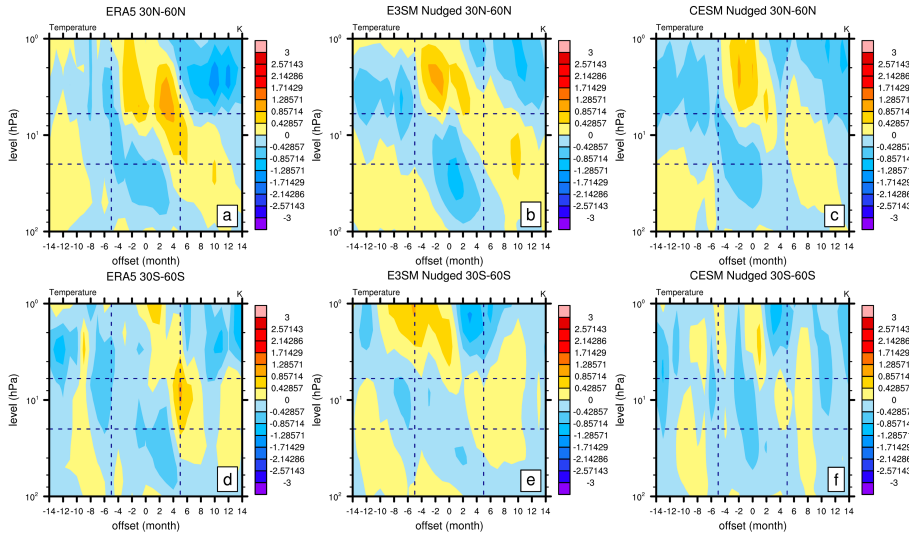
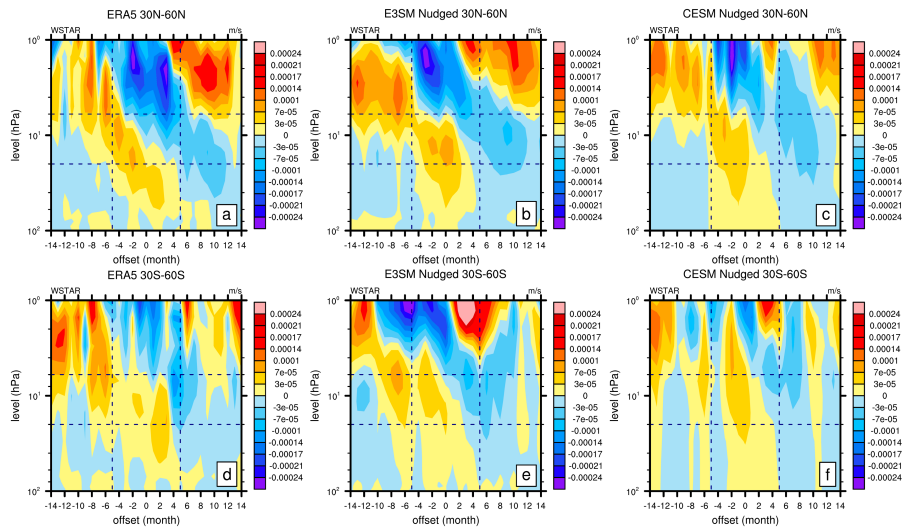


Figure 5 Pressure-time cross-section of the extra-tropical (30°N-60°N/30°S-60°S) temperature anomaly (K) as function of QBO phase for (a, d) ERA5, (b, e) E3SMv2, (c, f) CESM2 for 1979-2020. 0 is centered on the month when QBO index shifts from QBOe to QBOw (determined by when current QBO index < 0 and next QBO index > 0). The QBO phase is determined by 5S-5N average of the zonal wind.

Deleted: .
Deleted: anomalous
Deleted:



1211 **Figure 6** Pressure-time cross-section of the extratropical (30°N-60°N/30°S-60°S) w^* anomaly
1212 (m/s) as function of QBO for (a, d) ERA5, (b, e) E3SMv2 nudged, (c, f) CESM2 nudged for
1213 1979-2020. 0 is centered on the month when QBO index shifts from QBOe to QBOw
1214 (determined by when current QBO index<0 and next QBO index>0). The QBO phase is
1215 determined by 5S-5N average of the zonal wind.

Deleted: .

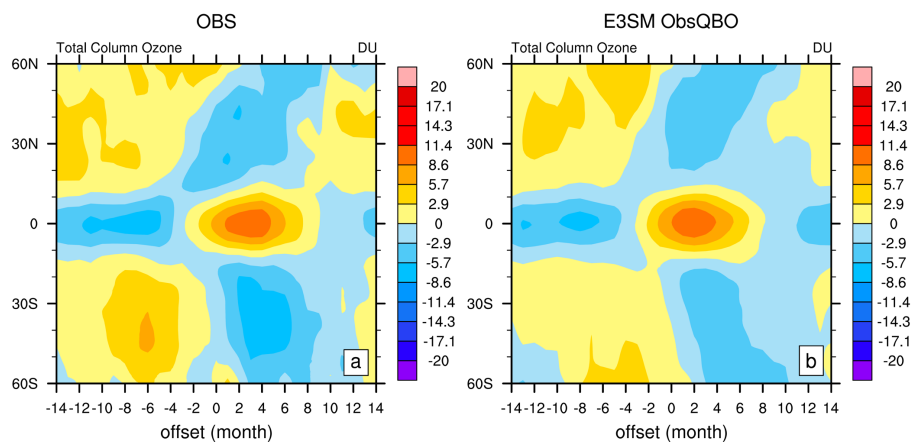


Figure 7 Total column ozone (TCO, Dobson Unit) anomaly (relative to 1979-2020 mean) composites as function of QBO phase (determined by NLPCA QBO index) for (a) OBS (Multi-Sensor Reanalysis version 2), (b) E3SMv2 nudged simulation for 1979-2020. 0 is centered on the month when QBO index shifts from QBOe to QBOw (determined by when current QBO index < 0 and next QBO index > 0). The QBO phase is determined by 5S-5N average of the zonal wind.

Deleted: .

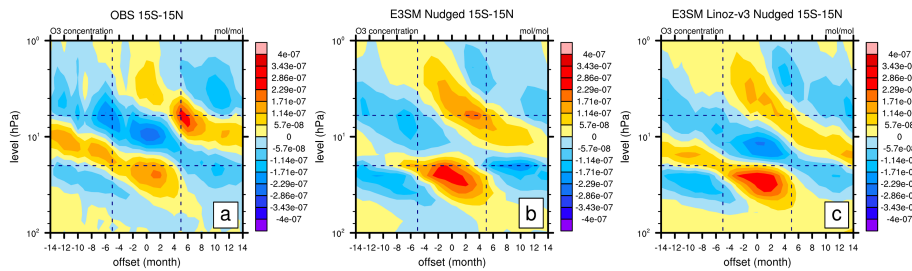


Figure 8 Pressure-time cross-section of the tropical (15°S-15°N) ozone concentration anomaly (mol/mol) as function of QBO phase for (a) Observation (Concentration Monthly Zonal Mean), (b) E3SMv2 nudged simulation, (c) E3SMv2 Linoz-v3 nudged simulation for 1979-2020. 0 is centered on the month when QBO index shifts from QBOe to QBOw (determined by when current QBO index < 0 and next QBO index > 0). The QBO phase is determined by 5S-5N average of the zonal wind. E3SMv2 Linoz-v3 nudged simulation is produced using nudged E3SMv2 with stratospheric chemistry replaced with Linoz-v3.

Deleted: .

Deleted: anomalous

Deleted: OBS

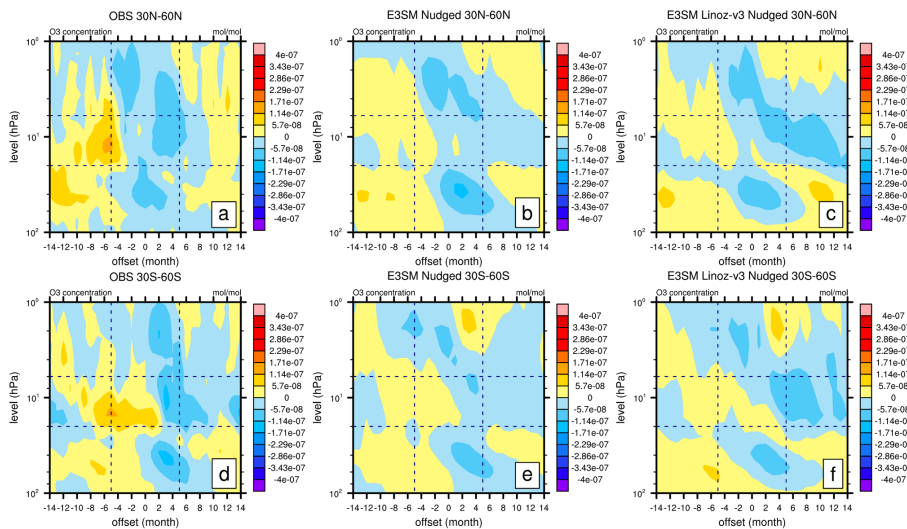


Figure 9 Pressure-time cross-section of the extratropical (30°N-60°N/30°S-60°S) ozone concentration anomaly (mol/mol) as function of QBO phase for (a, d) OBS (CMZM), (b, e) E3SMv2, (c, f) CESM2 for 1979-2020. 0 is centered on the month when QBO index shifts from QBOe to QBOw (determined by when current QBO index < 0 and next QBO index > 0). The QBO phase is determined by 5S-5N average of the zonal wind. E3SMv2 Linoz-v3 nudged simulation is produced using nudged E3SMv2 with stratospheric chemistry replaced with Linoz-v3.

Deleted: .

Deleted: anomalous

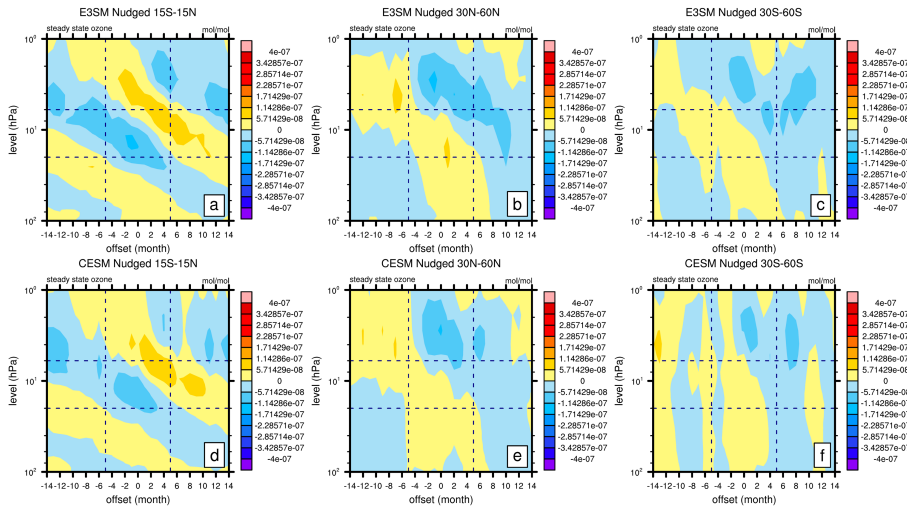


Figure 10 Pressure-time cross-section of the tropical (15°S-15°N) and extratropical (30°N-60°N/30°S-60°S) steady state ozone anomaly (mol/mol) as function of QBO phase for (a) E3SMv2 and (b) CESM2 for 1979-2020. 0 is centered on the month when QBO index shifts from QBOe to QBOw (determined by when current QBO index < 0 and next QBO index > 0). The QBO phase is determined by 5S-5N average of the zonal wind.

Deleted: .

Deleted: anomalous Linoz

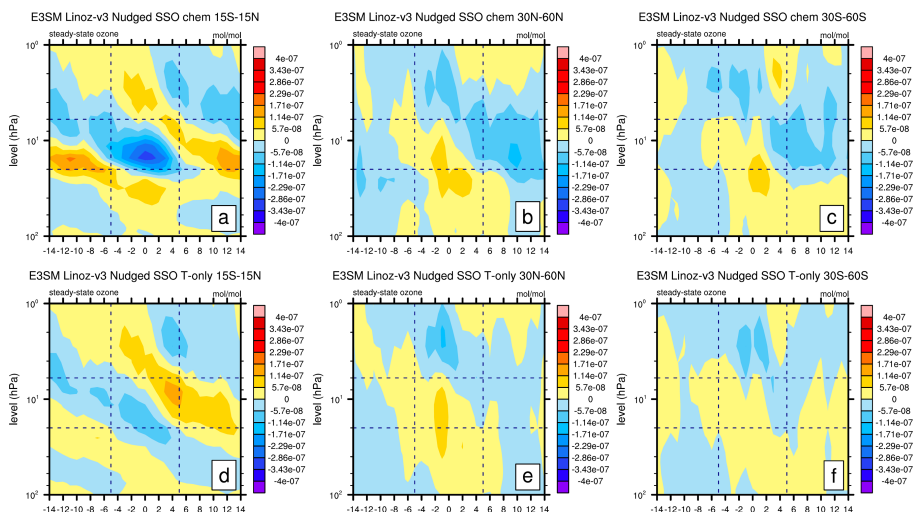


Figure 11 Pressure-time cross-section of the tropical (15°S-15°N) and extratropical (30°N-60°N/30°S-60°S) steady state ozone anomaly (mol/mol) as function of QBO for E3SMv2 Linoz-v3 Nudged simulation using (a, b, c) Linoz-v3 chemistry ($\text{NO}_y\text{-N}_2\text{O-CH}_4\text{-H}_2\text{O}$), (d, e, f) temperature only for 1979-2020. 0 is centered on the month when QBO index shifts from QBOc to QBOw (determined by when current QBO index < 0 and next QBO index > 0). The QBO phase is determined by 5S-5N average of the zonal wind.

Deleted: .

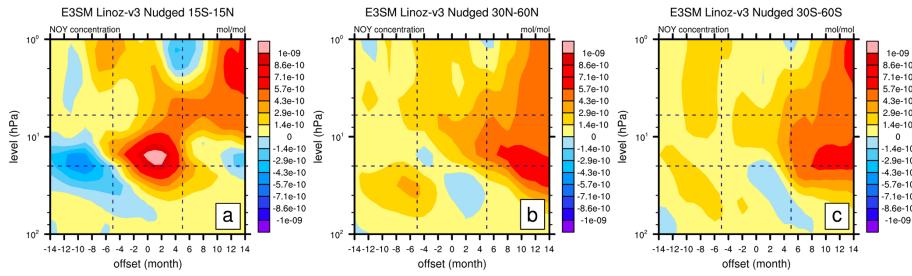


Figure 12 Pressure-time cross-section of the tropical (15°S-15°N) and extratropical (30°N-60°N/30°S-60°S) NO_y anomaly (mol/mol) as function of QBO (a, b, c) E3SMv2 Linoz-v3 for 1979-2020. 0 is centered on the month when QBO index shifts from QBO_e to QBO_w (determined by when current QBO index < 0 and next QBO index > 0). The QBO phase is determined by 5S-5N average of the zonal wind.

Deleted: .

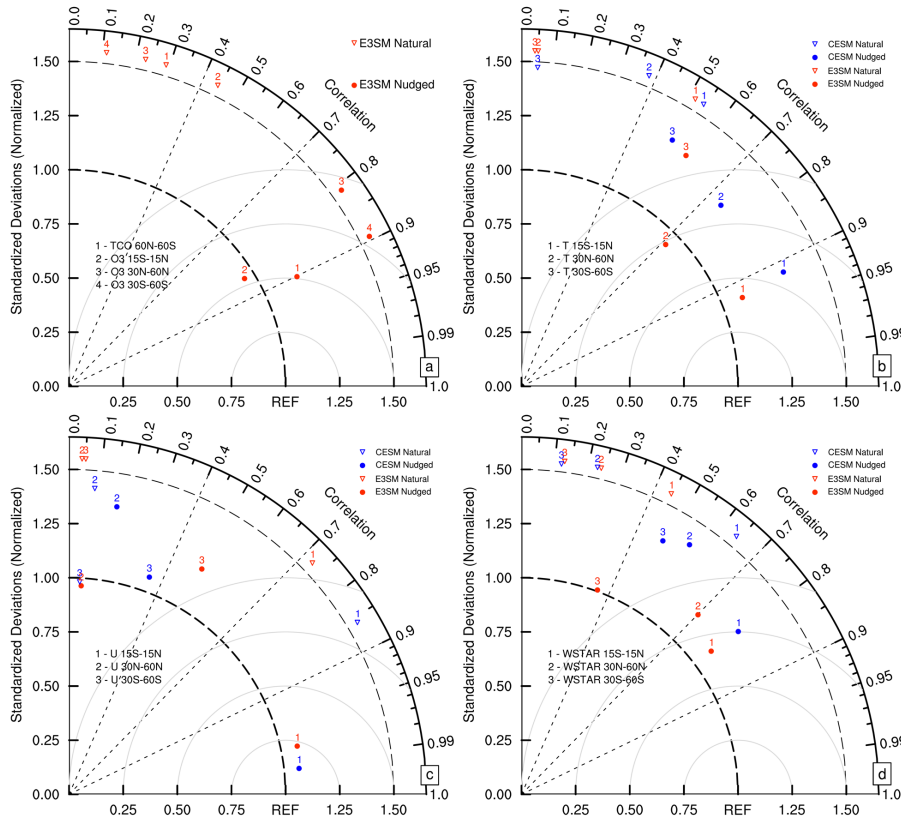


Figure 13 Taylor diagram of the E3SMv2/CESM2 simulation for various datasets for 1979-2020. (a) The area-weighted total column ozone (60°S - 60°N , DU) and pressure-time cross-sections of ozone concentration (15°S - 15°N , 30°N - 60°N , 30°S - 60°S , mol/mol) anomalies with OBS (MSR and CMZM), respectively. (b) The area-weighted pressure-time cross-sections of temperature (15°S - 15°N , 30°N - 60°N , 30°S - 60°S , K) anomalies with ERA5. (c) The area-weighted pressure-time cross-sections of zonal wind (15°S - 15°N , 30°N - 60°N , 30°S - 60°S , m/s) anomalies with ERA5. For pattern correlations, the cross-sections are weighted by pressure layer thickness. On all Taylor diagrams, the model standard deviations are normalized by dividing the standard deviations of the reference.

Deleted: .

Page 3: [1] Deleted

Jinbo Xie

3/7/25 10:42:00 PM



Page 3: [2] Deleted

Jinbo Xie

3/7/25 10:52:00 PM

